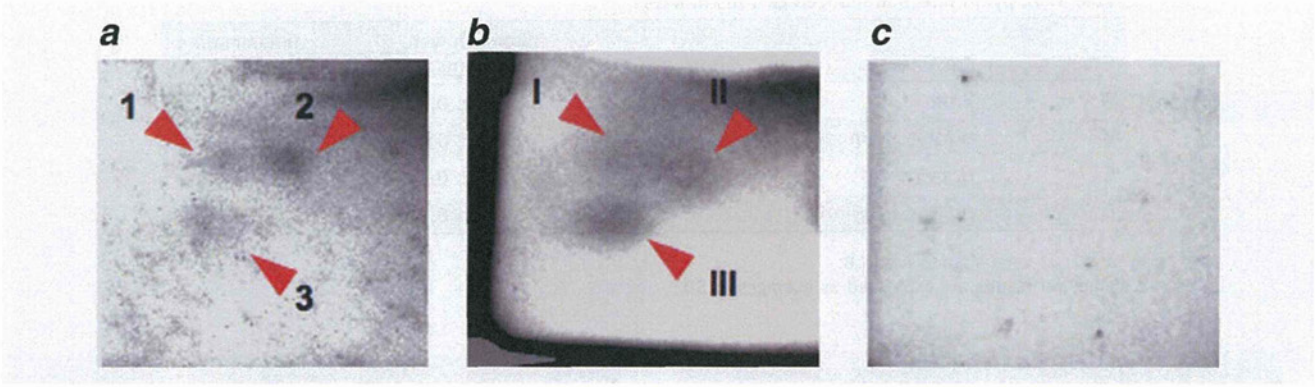

Figure 2. Autoradiograms of NIAN-DNA adducts in glandular stomach of MGs or calf thymus DNA treated with NIAN. Adducts were analyzed by ^{32}P-postlabeling method, as described in the Material and Methods. DNA samples were isolated from glandular stomach of MGs (*a*) or calf thymus DNA (*b*) after treatment with NIAN. DNA samples were also prepared from glandular stomach of MGs without NIAN treatment (*c*). Arrowheads indicate adducts. [Color figure can be viewed in the online issue, which is available at wileyonlinelibrary.com.]

animals of groups C and D were given an intragastric inoculation of *H. pylori* broth culture (0.5 ml, 0.9×10^8 CFU/animal) whereas animals of groups A and B were given sterilized broth alone (0.5 ml).[28]

During the experiments, animals which became moribund or emaciated (<80 g body weight) were sacrificed. At 104 weeks after *H. pylori* infection, all surviving animals were sacrificed under ether anesthesia. At performance of necropsy, all tissues were carefully checked macroscopically and the stomachs and major organs were removed and assessed for macroscopic lesion development. Effective numbers of animals were defined as those surviving until week 54 of the study, when gastric tumors were observed for the first time. In addition, in the *H. pylori*-infected groups, the animals developing gastritis observed on histological examination were regarded as effective. The percentages of gastritis-bearing animals by the single inoculation of *H. pylori* were 62% for group C and 76% for group D, being similar to those previously reported.[27] All animal experiments were performed according to the "Guidelines for Animal Experiments in the National Cancer Center" and were approved by the Institutional Ethics Review Committee for Animal Experimentation in the National Cancer Center.

Detection of DNA adducts by ^{32}P-postlabeling method

Calf thymus DNA (0.5 mg, Sigma, St. Louis, MO) treated with NIAN (3 mg) for 12 hr under neutral conditions was used for authentic NIAN-DNA adducts.[23] DNA samples from the glandular stomach of MGs and calf thymus DNA samples were digested with micrococcal nuclease and phosphodiesterase II, and subjected to ^{32}P-postlabeling analysis using the same procedure as described previously[23] except with solvent systems for two-dimensional development. The solvent system consisted of buffer A (4.0 M lithium formate, 7.7 M urea, pH 3.5) from bottom to top, and buffer B (0.90 M lithium chloride, 0.45 M Tris-HCl, 7.7 M urea, pH 8.0) from left to right, followed by 1.7 M sodium phosphate buffer, pH 6.0, from left to right, with 3.5 cm filter paper. Adducts were detected with a Bio-Image Analyzer (BAS 3000; Fuji Photo Film, Tokyo, Japan) after exposing the TLC sheets to Fuji imaging plates. Relative adduct labeling was determined by the methods of Reddy *et al.*,[29] and values were calculated as averages using data from three assays.

Histological examination

All excised stomachs were opened along the greater curvature and washed twice with saline, then fixed in 10% neutral-buffered formalin. The fixed stomachs were sliced along the longitudinal axis into 9–12 strips of equal width, and routinely processed to sections stained with hematoxylin and eosin (H&E). The degree of chronic active gastritis was graded according to criteria modified from the Updated Sydney System,[30] by scoring the infiltration of neutrophils and mononuclear cells. Other organs, in which macroscopic lesions were observed, were also fixed in 10% neutral-buffered formalin and routinely processed to sections stained with H&E for histological examination.

Statistical analysis

The significance of differences in quantitative data for gastric inflammation, gastric adenocarcinoma and tumors of other organs was analyzed by Fisher's exact test. Data for stomach wet weight and inflammation score were examined using Tukey's multiple comparison test. Significance was concluded at $p < 0.05$.

Results

DNA adduct formation by NIAN administration in the glandular stomach of MGs

To confirm the formation of NIAN-DNA adducts in the glandular stomach of MGs, NIAN was injected two times a week at a dose of 100 mg/kg by gavage, and then analyzed by ^{32}P-postlabeling method. Three adduct spots were observed in DNA samples derived from NIAN-treated animals (Fig. 2*a*). The adduct levels were 0.3 for adduct 1, 1.1 for adduct 2, 0.2 for adduct 3 and 1.6 adducts/10^8 nucleotides

Table 1. *H. pylori* infection induced-gastritis in MGs

Group	Treatment	Effective No.	Stomach wet weight (g)	Inflammation score
A	Broth	15	0.647 ± 0.097	0
B	NIAN + Broth	22	0.631 ± 0.094	0
C	*H. pylori*	18	1.432 ± 0.445*	2.22 ± 0.43*
D	NIAN + *H. pylori*	26	1.483 ± 0.445*	2.38 ± 0.64*

*$p < 0.01$ versus group A and B.
Values for results are expressed as averages ± SD.

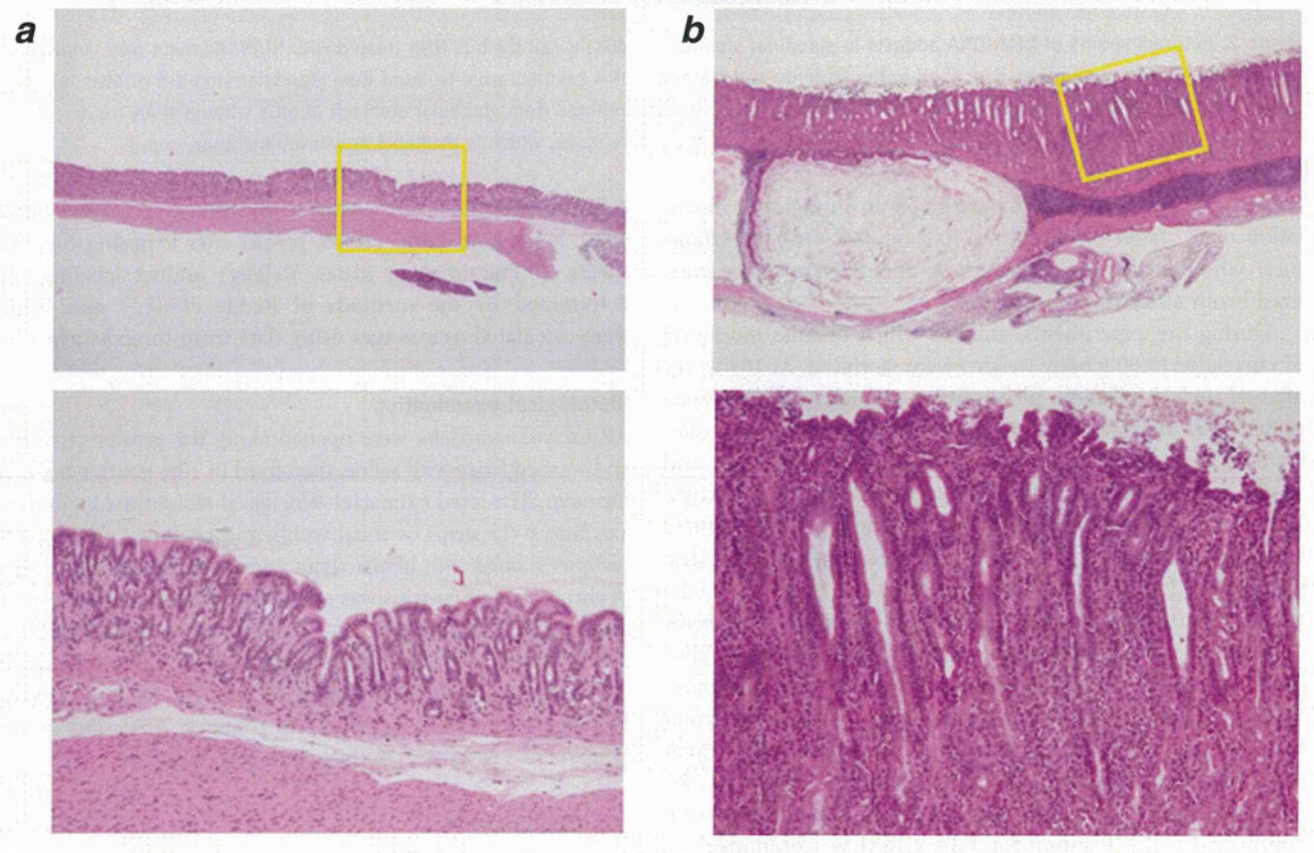

Figure 3. Macroscopic and microscopic views of gastritis in MGs infected or uninfected with *H. pylori*. (*a*) Normal gastric mucosa in group A. (*b*) Severe infiltration of many inflammatory cells with development of heterophilic proliferative glands in group C; H&E staining, ×40. Yellow boxes are shown at greater magnification below, ×200.

in total. This TLC pattern was similar to that in the *in vitro* reaction of calf thymus DNA with NIAN (total adduct level of 4.8 adducts/10^7 nucleotides, Fig. 2*b*). In the case of DNA samples derived from control animals, no adduct spots were seen on the TLC sheets (Fig. 2*c*).

Macroscopical and microscopical observation of *H. pylori*-induced gastritis in MGs

MGs were sacrificed until 104 weeks after *H. pylori* infection, and gastric disorders were analyzed. Stomach wet weights and gastric inflammation scores are shown in Table 1. Macroscopically, edematous thickening with hemorrhagic spots was apparent in the gastric mucosa in *H. pylori*-infected MGs (groups C and D), but not in animals uninfected with *H. pylori* (groups A and B). The stomach wet weight, reflecting edematous thickening, in animals infected with *H. pylori* (groups C and D) was significantly increased compared with that of animals not infected with *H. pylori* (groups A and B) ($p < 0.01$). No significant differences of stomach wet weight were detected between groups A and B and also between groups C and D.

Microscopically, gastritis, featuring infiltration of many inflammatory cells, and hyperplastic change of glandular epithelium, and erosion were observed in the pyloric regions of

Table 2. Incidence of glandular stomach adenocarcinoma in MGs

Group	Treatment	Effective No.	No. of animals with glandular stomach adenocarcinoma (%)		
			Total	Well dif.	Moderately dif.
A	Broth	15	0 (0)	0 (0)	0 (0)
B	NIAN + Broth	22	0 (0)	0 (0)	0 (0)
C	*H. pylori*	18	0 (0)	0 (0)	0 (0)
D	NIAN + *H. pylori*	26	8 (31)*	7 (27)	1 (4)

Well dif., well differentiated adenocarcinoma; Moderately dif., moderately differentiated adenocarcinoma.
*$p < 0.05$ versus group A and C and $p < 0.01$ versus group B.

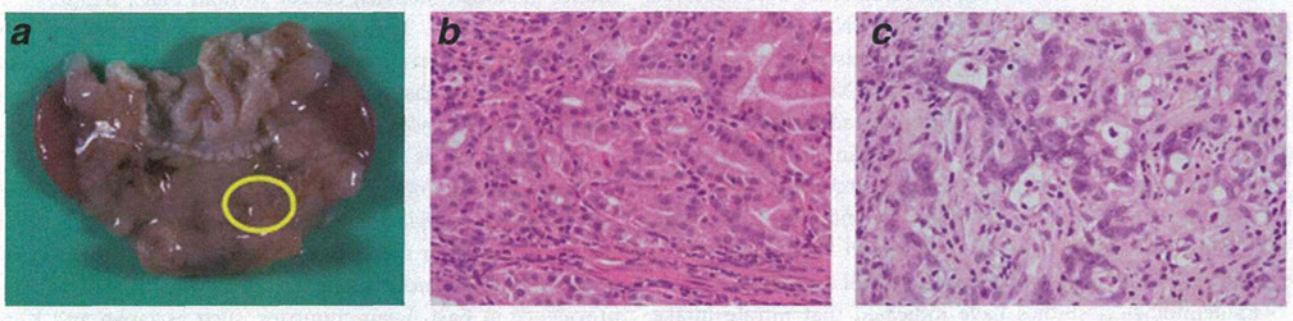

Figure 4. Histological findings of gastric adenocarcinoma in the animals treated with both NIAN and *H. pylori*. (*a*) Typical macrograph of a stomach. The yellow circle shows the suspected lesion of gastric cancer. (*b*) Well differentiated adenocarcinoma. (*c*) Moderately differentiated adenocarcinoma. (*b* and *c*) H&E staining, ×400.

the animals infected with *H. pylori* (groups C and D) (Fig. 3). Heterotopic proliferative glands, whose development is related to severe gastritis in *H. pylori*-infected MGs, were sometimes observed in *H. pylori*-infected groups (groups C and D). No gastritis was found in animals not infected with *H. pylori* (groups A and B). The gastric inflammation score in *H. pylori*-infected animals was significantly increased compared with that of animals uninfected with *H. pylori* ($p < 0.01$). There were no significant differences of gastric inflammation score between groups C and D.

Development of glandular stomach adenocarcinomas in MGs treated with both NIAN and *H. pylori*

The observed incidences of glandular stomach adenocarcinomas are shown in Table 2. Glandular stomach adenocarcinomas, histologically featuring tubular structures with cellular atypia infiltrating into the muscle layer, were found in eight animals treated with both NIAN and *H. pylori* (8/26 = 31%) at 54–104 weeks. All adenocarcinomas were observed in the pyloric mucosa and located in the lesser curvature of the stomach, where macroscopically severe edematous thickening was also seen (Fig. 4*a*). The observed adenocarcinomas in seven animals were of well differentiated (Fig. 4*b*), and a moderately differentiated lesion was observed in one animal (Fig. 4*c*). In the animals treated with broth alone, broth + NIAN and *H. pylori* alone (groups A, B and C), no glandular stomach adenocarcinomas were observed. The incidence of glandular stomach adenocarcinomas in group D was significantly higher than that in groups A, B and C ($p < 0.05$, $p < 0.01$ and $p < 0.05$, respectively).

Irrespective of NIAN treatment and *H. pylori* infection, skin tumors, which histologically were well to poor differentiated squamous cell carcinomas, sebaceous carcinomas and melanomas, were found in one animal (1/15 = 7%) in group A, three animals (3/22 = 14%) in group B, two animals (2/18 = 11%) in group C and five animals (5/26 = 19%) in group D. A hemangioma was also observed in a kidney of one animal in group D (1/26 = 4%). No significant differences were apparent in these tumor incidences among groups A–D.

Discussion

In the present study, NIAN was found to induce glandular stomach adenocarcinomas in MGs in combination with *H. pylori* infection. NIAN-DNA adducts were also detected in the glandular stomach of MGs after treatment with NIAN, although clarification of their chemical structure(s) has yet to be performed. DNA adducts observed in the glandular stomachs of NIAN-treated MGs probably contain an indole-3-acetonitrile moiety. However, it is further likely that NIAN would act as an NO donor under aqueous conditions, thereby causing DNA modifications.[31–33] In fact, Lucas *et al.* demonstrated that NIAN can efficiently transfer nitroso groups to nucleophilic targets in purine nucleotides, causing *N*-nitrosation, deamination and the formation of a novel guanine analog, oxanine.[33]

Glandular stomach adenocarcinomas induced by NIAN treatment plus *H. pylori* infection were located in the pyloric region, similar to MNNG or MNU treatment plus *H. pylori* infection-induced glandular stomach adenocarcinomas in MGs.[26,27] Meanwhile, no glandular stomach cancers were observed in the groups of *H. pylori*-infected MGs without NIAN treatment, which is consistent with previous studies,[26,27] nor in the group treated with only NIAN. These findings indicated that *H. pylori* is a strong promoter of gastric carcinogenesis. Histological examination revealed that the tumors developed by NIAN + *H. pylori* were of well or moderately differentiated adenocarcinomas. Well or poorly differentiated adenocarcinomas and signet ring cell carcinomas were observed in *H. pylori*-infected MGs treated with MNNG or MNU.[26,27] Further studies are required to clarify the histological variety of stomach adenocarcinomas induced by NIAN, MNNG or MNU, since the type of cancer might depend on the genotoxic action of chemical carcinogens, rather than the effects of *H. pylori* infection.[27] In addition, tumors were observed in skin and kidney, which were suspected to spontaneously develop. The MGs have been reported to develop spontaneous skin tumors such as sebaceous and squamous cell carcinoma.[34]

Epidemiological studies have indicated that nitrate intake increases gastric cancer risk, and major sources are vegetables including Chinese cabbage, spinach and parsley.[14] Indole-3-acetonitrile, a precursor of NIAN, is distributed widely in cruciferous vegetables including Chinese cabbage and sprouts.[35] Furthermore, fava beans (*Vicia faba*), which are commonly consumed in Colombia, give rise to a potent mutagen in the presence of nitrite under acidic conditions.[36] The nitrosatable precursor of the mutagen in fava beans and the major product of nitrosation are reported to be an indole compound, 4-chloro-6-methoxyindole and an *N*-nitroso compound, 4-chloro-2-hydroxy-N^1-nitroso-indolin-3-one oxime, respectively.[37] Other indole compounds are also reported to produce direct-acting mutagens after nitrite treatment under acidic conditions.[38,39] In general, conversion of indole derivatives to nitrosated forms *in vitro* is known to be rapid and efficient at physiologically feasible nitrite concentrations with the low pH of the human stomach.[37] Thus, it is conceivable that nitrosation of indole compounds such as indole-3-acetonitrile probably occurs in human stomach. On the other hand, nitric oxide is suggested to be produced by activated macrophages in inflamed organs with *H. pylori* infection.[18] Therefore, nitrosation of indole compounds could be mediated by both acid catalysis and inflammatory responses in the human stomach.[18,20,37–40] On the basis of the conversion rate of NIAN from indole-3-acetonitrile under physiological conditions, the dose of NIAN used in the present study appears about 500–1000 fold the expected human exposure to NIAN *via* fresh or pickled Chinese cabbage. However, humans continually consume various kinds of foods containing indole compounds and nitrate during ordinary life. Thus, it is probable that the total amount of nitroso-indole compounds would be much closer to the dose of NIAN used in the present study. Moreover, it has been reported that low doses of chemical carcinogens, such as MNNG and MNU, could induce glandular stomach cancers in rodents under inflammation conditions including NaCl treatment and *H. pylori* infection, but hardly induce glandular stomach cancer without NaCl treatment and *H. pylori* infection. Therefore, the continuous intake of indole compounds and nitrate may play an important role for gastric carcinogenesis in East Asian countries still with a high salt consumption and *H. pylori* infection rate.

Gastric cancer is tending to decline in most countries.[41–43] One of the explanations for this tendency is the reduced prevalence of *H. pylori* infection.[42] Changes in dietary habits, mainly being lower salt consumption, could be also related to reduced gastric cancer incidence. However, the gastric cancer prevalence in East Asian countries, such as Japan and Korea, is still high.[2] At present, we have not succeeded in detecting NIAN in human bodies nor the exposure levels of the precursor, indole compounds for humans. Thus, it is necessary to estimate the human exposure levels to nitroso-indole compounds including NIAN, and to study further animal experiments and epidemiological analyses for clarification of contribution of nitroso-indole compounds under *H. pylori* infection in humans gastric carcinogenesis.

In conclusion, the present study demonstrated that NIAN can induce gastric cancer in *H. pylori*-infected MGs. It is noteworthy that nitrosatable precursors widely exist in foods. Thus, it is suggested that *N*-nitroso indole compounds including NIAN might contribute to the frequent development of gastric cancer in East Asian countries such as Japan and Korea in which the prevalence of *H. pylori* infection is relatively high. Further studies of interaction with other dietary elements appear warranted to promote the prevention of human gastric cancer.

Acknowledgements

The authors thank Dr. Nobuo Takasuka, Naoaki Uchiya and Yusaku Hori for their expert technical assistance. S.T. is presently the recipient of a Research Resident Fellowship from the Foundation for Promotion of Cancer Research.

References

1. Boyle P, Ferlay J. Cancer incidence and mortality in Europe, 2004. *Ann Oncol* 2005;16:481–8.
2. Bertuccio P, Chatenoud L, Levi F, Praud D, Ferlay J, Negri E, Malvezzi M, La Vecchia C. Recent patterns in gastric cancer: a global overview. *Int J Cancer* 2009;125:666–73.
3. Tsugane S, Sasazuki S. Diet and the risk of gastric cancer: review of epidemiological evidence. *Gastric Cancer* 2007;10:75–83.
4. Parsonnet J, Friedman GD, Vandersteen DP, Chang Y, Vogelman JH, Orentreich N, Sibley RK. Helicobacter pylori infection and the risk of gastric carcinoma. *N Engl J Med* 1991;325:1127–31.

5. Uemura N, Okamoto S, Yamamoto S, Matsumura N, Yamaguchi S, Yamakido M, Taniyama K, Sasaki N, Schlemper RJ. Helicobacter pylori infection and the development of gastric cancer. *N Engl J Med* 2001;345:784–9.
6. Parkin DM. The global health burden of infection-associated cancers in the year 2002. *Int J Cancer* 2006;118:3030–44.
7. Yim JY, Kim N, Choi SH, Kim YS, Cho KR, Kim SS, Seo GS, Kim HU, Baik GH, Sin CS, Cho SH, Oh BH. Seroprevalence of Helicobacter pylori in South Korea. *Helicobacter* 2007;12:333–40.
8. Tajima K, Tominaga S. Dietary habits and gastro-intestinal cancers: a comparative case-control study of stomach and large intestinal cancers in Nagoya, Japan. *Jpn J Cancer Res* 1985;76:705–16.
9. Kim HJ, Chang WK, Kim MK, Lee SS, Choi BY. Dietary factors and gastric cancer in Korea: a case-control study. *Int J Cancer* 2002;97:531–5.
10. Nan HM, Park JW, Song YJ, Yun HY, Park JS, Hyun T, Youn SJ, Kim YD, Kang JW, Kim H. Kimchi and soybean pastes are risk factors of gastric cancer. *World J Gastroenterol* 2005;11:3175–81.
11. Seel DJ, Kawabata T, Nakamura M, Ishibashi T, Hamano M, Mashimo M, Shin SH, Sakamoto K, Jhee EC, Watanabe S. N-Nitroso compounds in two nitrosated food products in southwest Korea. *Food Chem Toxicol* 1994;32:1117–23.
12. Jakszyn P, Bingham S, Pera G, Agudo A, Luben R, Welch A, Boeing H, Del Giudice G, Palli D, Saieva C, Krogh V, Sacerdote C, *et al.* Endogenous *versus* exogenous exposure to N-nitroso compounds and gastric cancer risk in the European Prospective Investigation into Cancer and Nutrition (EPIC-EURGAST) study. *Carcinogenesis* 2006;27:1497–501.
13. Joossens JV, Hill MJ, Elliott P, Stamler R, Lesaffre E, Dyer A, Nichols R, Kesteloot H. Dietary salt, nitrate and stomach cancer mortality in 24 countries. European Cancer Prevention (ECP) and the INTERSALT Cooperative Research Group. *Int J Epidemiol* 1996;25:494–504.
14. van Velzen AG, Sips AJ, Schothorst RC, Lambers AC, Meulenbelt J. The oral bioavailability of nitrate from nitrate-rich vegetables in humans. *Toxicol Lett* 2008; 181:177–81.
15. Spiegelhalder B, Eisenbrand G, Preussmann R. Influence of dietary nitrate on nitrite content of human saliva: possible relevance to *in vivo* formation of N-nitroso compounds. *Food Cosmet Toxicol* 1976;14: 545–8.
16. Sugimura T, Fujimura S. Tumour production in glandular stomach of rat by N-methyl-N′-nitro-N-nitrosoguanidine. *Nature* 1967;216:943–4.
17. Hirota N, Aonuma T, Yamada S, Kawai T, Saito K, Yokoyama T. Selective induction of glandular stomach carcinoma in F344 rats by N-methyl-N-nitrosourea. *Jpn J Cancer Res* 1987;78:634–8.
18. Ohshima H, Bartsch H. Chronic infections and inflammatory processes as cancer risk factors: possible role of nitric oxide in carcinogenesis. *Mutat Res* 1994;305:253–64.
19. Wakabayashi K, Nagao M, Ochiai M, Tahira T, Yamaizumi Z, Sugimura T. A mutagen precursor in Chinese cabbage, indole-3-acetonitrile, which becomes mutagenic on nitrite treatment. *Mutat Res* 1985;143:17–21.
20. Wakabayashi K, Nagao M, Ochiai M, Fujita Y, Tahira T, Nakayasu M, Ohgaki H, Takayama S, Sugimura T. Recently identified nitrite-reactive compounds in food: occurrence and biological properties of the nitrosated products. *IARC Sci Publ* 1987:287–91.
21. Wakabayashi K, Nagao M, Tahira T, Saito H, Katayama M, Marumo S, Sugimura T. 1-Nitrosoindole-3-acetonitrile, a mutagen produced by nitrite treatment of indole-3-acetonitrile. *Proc Jpn Acad Ser* 1985;B61: 190–92.
22. Tiedink HG, Davies JA, Visser NA, Jongen WM, van Broekhoven LW. The stability of the nitrosated products of indole, indole-3-acetonitrile, indole-3-carbinol and 4-chloroindole. *Food Chem Toxicol* 1989; 27:723–30.
23. Yamashita K, Wakabayashi K, Kitagawa Y, Nagao M, Sugimura T. ^{32}P-postlabeling analysis of DNA adducts in rat stomach with 1-nitrosoindole-3-acetonitrile, a direct-acting mutagenic indole compound formed by nitrosation. *Carcinogenesis* 1988; 9:1905–7.
24. Furihata C, Ikui E, Matsushima T. DNA single-strand scission in the pyloric mucosa of rat stomach induced by four glandular stomach carcinogens and three other chemicals. *Mutat Res* 1996; 368:1–6.
25. Tatematsu M, Yamamoto M, Iwata H, Fukami H, Yuasa H, Tezuka N, Masui T, Nakanishi H. Induction of glandular stomach cancers in C3H mice treated with N-methyl-N-nitrosourea in the drinking water. *Jpn J Cancer Res* 1993;84: 1258–64.
26. Sugiyama A, Maruta F, Ikeno T, Ishida K, Kawasaki S, Katsuyama T, Shimizu N, Tatematsu M. Helicobacter pylori infection enhances N-methyl-N-nitrosourea-induced stomach carcinogenesis in the Mongolian gerbil. *Cancer Res* 1998;58:2067–9.
27. Shimizu N, Inada K, Nakanishi H, Tsukamoto T, Ikehara Y, Kaminishi M, Kuramoto S, Sugiyama A, Katsuyama T, Tatematsu M. Helicobacter pylori infection enhances glandular stomach carcinogenesis in Mongolian gerbils treated with chemical carcinogens. *Carcinogenesis* 1999;20: 669–76.
28. Matsubara S, Shibata H, Ishikawa F, Yokokura T, Takahashi M, Sugimura T, Wakabayashi K. Suppression of Helicobacter pylori-induced gastritis by green tea extract in Mongolian gerbils. *Biochem Biophys Res Commun* 2003;310: 715–9.
29. Reddy MV, Randerath K. Nuclease P1-mediated enhancement of sensitivity of ^{32}P-postlabeling test for structurally diverse DNA adducts. *Carcinogenesis* 1986;7: 1543–51.
30. Dixon MF, Genta RM, Yardley JH, Correa P. Classification and grading of gastritis. The updated Sydney System. International Workshop on the Histopathology of Gastritis, Houston 1994. *Am J Surg Pathol* 1996;20:1161–81.
31. Lucas LT, Gatehouse D, Shuker DE. Efficient nitroso group transfer from N-nitrosoindoles to nucleotides and 2′-deoxyguanosine at physiological pH. A new pathway for N-nitrosocompounds to exert genotoxicity. *J Biol Chem* 1999;274: 18319–26.
32. Burney S, Caulfield JL, Niles JC, Wishnok JS, Tannenbaum SR. The chemistry of DNA damage from nitric oxide and peroxynitrite. *Mutat Res* 1999;424:37–49.
33. Lucas LT, Gatehouse D, Jones GD, Shuker DE. Characterization of DNA damage at purine residues in oligonucleotides and calf thymus DNA induced by the mutagen 1-nitrosoindole-3-acetonitrile. *Chem Res Toxicol* 2001;14:158–64
34. Vincent AL, Ash LR. Further observations on spontaneous neoplasms in the Mongolian gerbil, Meriones unguiculatus. *Lab Anim Sci* 1978;28:297–300.
35. Okamoto T, Isogai Y, Koizumi T, Fujishiro H, Sato Y. Studies on plant growth regulators, III. Isolation of indole-3-acetonitrile and methyl indole-3-acetate from the neutral fraction of the Moyashi extract. *Chem Pharm Bull* 1967;15: 163–68.
36. Piacek-Llanes BG, Tannenbaum SR. Formation of an activated N-nitroso compound in nitrite-treated fava beans (Vicia faba). *Carcinogenesis* 1982;3: 1379–84.
37. Yang D, Tannenbaum SR, Buchi G, Lee GC. 4-Chloro-6-methoxyindole is the precursor of a potent mutagen (4-chloro-6-methoxy-2-hydroxy-1-nitroso-indolin-3-one oxime) that forms during nitrosation of the fava bean (Vicia faba). *Carcinogenesis* 1984;5:1219–24.
38. Ochiai M, Wakabayashi K, Sugimura T, Nagao M. Mutagenicities of indole and 30 derivatives after nitrite treatment. *Mutat Res* 1986;172:189–97.

39. Wakabayashi K, Ochiai M, Saito H, Tsuda M, Suwa Y, Nagao M, Sugimura T. Presence of 1-methyl-1,2,3,4-tetrahydro-beta-carboline-3-carboxylic acid, a precursor of a mutagenic nitroso compound, in soy sauce. *Proc Natl Acad Sci USA* 1983;80:2912–6.
40. Suzuki T, Mower HF, Friesen MD, Gilibert I, Sawa T, Ohshima H. Nitration and nitrosation of N-acetyl-L-tryptophan and tryptophan residues in proteins by various reactive nitrogen species. *Free Radic Biol Med* 2004;37:671–81.
41. Inoue M, Tsugane S. Epidemiology of gastric cancer in Japan. *Postgrad Med J* 2005;81:419–24.
42. Kobayashi T, Kikuchi S, Lin Y, Yagyu K, Obata Y, Ogihara A, Hasegawa A, Miki K, Kaneko E, Mizukoshi H, Sakiyama T, Tenjin H. Trends in the incidence of gastric cancer in Japan and their associations with Helicobacter pylori infection and gastric mucosal atrophy. *Gastric Cancer* 2004;7:233–9.
43. Plummer M, Franceschi S, Munoz N. Epidemiology of gastric cancer. *IARC Sci Publ* 2004;157:311–26.

Cancer Science
The official journal of the Japanese Cancer Association

Multi-walled carbon nanotubes translocate into the pleural cavity and induce visceral mesothelial proliferation in rats

Jiegou Xu,[1,2] Mitsuru Futakuchi,[2] Hideo Shimizu,[3] David B. Alexander,[1] Kazuyoshi Yanagihara,[4] Katsumi Fukamachi,[2] Masumi Suzui,[2] Jun Kanno,[5] Akihiko Hirose,[6] Akio Ogata,[7] Yoshimitsu Sakamoto,[7] Dai Nakae,[7] Toyonori Omori[8] and Hiroyuki Tsuda[1,9]

[1]Laboratory of Nanotoxicology Project, Nagoya City University, Nagoya; [2]Department of Molecular Toxicology; [3]Core Laboratory, Nagoya City University Graduate School of Medical Sciences, Nagoya; [4]Department of Life Sciences, Yasuda Women's University Faculty of Pharmacy, Hiroshima; [5]Division of Cellular and Molecular Toxicology; [6]Division of Risk Assessment, National Institute of Health Sciences, Tokyo; [7]Department of Pharmaceutical and Environmental Sciences, Tokyo Metropolitan Institute of Public Health, Tokyo; [8]Department of Health Care Policy and Management, Nagoya City University Graduate School of Medical Sciences, Nagoya, Japan

(Received July 17, 2012/Revised August 20, 2012/Accepted August 22, 2012/Accepted manuscript online August 31, 2012/Article first published online October 10, 2012)

Multi-walled carbon nanotubes have a fibrous structure similar to asbestos and induce mesothelioma when injected into the peritoneal cavity. In the present study, we investigated whether carbon nanotubes administered into the lung through the trachea induce mesothelial lesions. Male F344 rats were treated with 0.5 mL of 500 μg/mL suspensions of multi-walled carbon nanotubes or crocidolite five times over a 9-day period by intrapulmonary spraying. Pleural cavity lavage fluid, lung and chest wall were then collected. Multi-walled carbon nanotubes and crocidolite were found mainly in alveolar macrophages and mediastinal lymph nodes. Importantly, the fibers were also found in the cell pellets of the pleural cavity lavage, mostly in macrophages. Both multi-walled carbon nanotube and crocidolite treatment induced hyperplastic proliferative lesions of the visceral mesothelium, with their proliferating cell nuclear antigen indices approximately 10-fold that of the vehicle control. The hyperplastic lesions were associated with inflammatory cell infiltration and inflammation-induced fibrotic lesions of the pleural tissues. The fibers were not found in the mesothelial proliferative lesions themselves. In the pleural cavity, abundant inflammatory cell infiltration, mainly composed of macrophages, was observed. Conditioned cell culture media of macrophages treated with multi-walled carbon nanotubes and crocidolite and the supernatants of pleural cavity lavage fluid from the dosed rats increased mesothelial cell proliferation *in vitro*, suggesting that mesothelial proliferative lesions were induced by inflammatory events in the lung and pleural cavity and likely mediated by macrophages. In conclusion, intrapulmonary administration of multi-walled carbon nanotubes, like asbestos, induced mesothelial proliferation potentially associated with mesothelioma development. (*Cancer Sci* 2012; 103: 2045–2050)

Multi-walled carbon nanotubes (MWCNT) are structurally composed of cylinders rolled up from several layers of graphite sheets. They are several to tens of nanometers in diameter and several to tens of micrometers in length. This high length to diameter aspect ratio, a characteristic shared with asbestos fibers, has led to concern that exposure to MWCNT might cause asbestos-like lung diseases, such as lung fibrosis, lung cancer, pleural plaque and malignant mesothelioma.[1–6]

Pleural plaque and malignant mesothelioma are characteristic lesions in asbestos-exposed humans. Although fiber dimensions, biopersistence, oxidative stress and inflammation have all been implicated,[7–12] the exact mechanisms of pleural pathogenesis are unclear. According to a pathogenesis paradigm suggested by Donaldson *et al.*,[2] asbestos fibers penetrate into the pleural cavity from the alveoli and deposit in the pleural tissue. Unlike spherical particles, fibrous materials such as asbestos are not cleared effectively from the pleural cavity, resulting in deposition of the fibers in the parietal pleura. This deposition, in turn, causes frustrated phagocytosis-induced pro-inflammatory, genotoxic and mitogenic responses in the deposition sites.[2]

Administration of MWCNT into the peritoneal cavity or scrotum in animals has been reported to induce mesothelial lesions, similar to those observed in asbestos cases.[13–15] The induction of mesothelioma in the peritonum is dose dependent, and is observed with as low as 3 μg/mouse in p53 heterozygous mice.[16] These studies suggest a potential risk that inhaled MWCNT might lead to pleural mesothelioma. However, actual experimental evidence demonstrating induction of pleural mesothelioma by inhaled MWCNT fibers has not yet been shown. It has been shown that inhaled MWCNT induced subpleural fibrosis with macrophage aggregates on the surface of the visceral pleura.[17] Notably, some of these macrophages contained MWCNT fibers. In addition, penetration of MWCNT administrated by pharyngeal aspiration into the pleural cavity was observed,[18] and intrapleural injection of 5 μg/mouse of MWCNT has been shown to lead to sustained inflammation and length-dependent retention of MWCNT in the pleural cavity.[19] Accordingly, direct interaction of MWCNT with the mesothelial tissue is postulated as an early pathogenic event.

In the present study, to examine whether MWCNT translocate into the pleural cavity and cause inflammation leading to proliferative change of the mesothelial tissue, we administered relatively high doses (five doses at 250 μg/rat) of two MWCNT samples (MWCNT-N and MWCNT-M) to the rat lung by intrapulmonary spraying (IPS)/intratracheal instillation; crocidolite (CRO; one kind of asbestos fiber) was used as a positive control. Intrapulmonary spraying has been shown to be an efficient method to deliver particle materials deep into the lung.[20–24] Our results demonstrated that MWCNT, like asbestos, translocated from the lung into the pleural cavity and induced inflammatory responses in the pleural cavity and, importantly, hyperplastic visceral mesothelial proliferation. These findings are important in understanding whether MWCNT have the potential to cause asbestos-like pleural lesions.

[9]To whom correspondence should be addressed.
E-mail: htsuda@phar.nagoya-cu.ac.jp

doi: 10.1111/cas.12005

Materials and Methods

Animals. Eight-week-old male F344 rats were purchased from Charles River Japan Inc. (Kanagawa, Japan). The animals were housed in the Animal Center of Nagoya City University Medical School and maintained on a 12 h light/12 h dark cycle, and received Oriental MF basal diet (Oriental Yeast Co. Ltd, Tokyo, Japan) and water *ad libitum*. The study was conducted according to the Guidelines for the Care and Use of Laboratory Animals of Nagoya City University Medical School and the experimental protocol was approved by the Institutional Animal Care and Use Committee (H22M-19).

Preparation of MWCNT and CRO suspensions. The MWCNT investigated were MWCNT-N (Nikkiso Co., Ltd, Tokyo, Japan) and MWCNT-7 (Mitsui Chemicals Inc., Tokyo, Japan; designated as MWCNT-M). Crocidolite (Union for International Cancer Control grade) was from the National Institute of Health Sciences of Japan stocks. Ten milligrams of MWCNT-N or MWCNT-M were suspended in 20 mL of saline containing 0.1% Tween 20 and homogenized for 1 min four times at 3000 r.p.m. in a Polytron PT1600E benchtop homogenizer (Kinematika AG, Littau, Switzerland). The suspensions were sonicated for 30 min shortly before use to minimize aggregation. The CRO suspension was prepared similarly, but without homogenization. The concentration of the MWCNT and CRO suspensions was 500 μg/mL. The lengths of MWCNT and CRO in the suspensions were determined using a digital map meter (Comcureve-9 Junior; Koizumi Sokki MFG. Co., Ltd, Nigata, Japan) on scanning electron microscope (SEM) photos. The SEM observation and length distributions of MWCNT and CRO are shown in Fig. S1A,B. To count the fiber number, 500 μg/mL suspensions of MWCNT-N, MWCNT-M and CRO were diluted 1:1000 with deionized water and 0.5 μL of the diluted suspensions was loaded onto clean glass slides and dried in a micro oven at 480°C for 1 min. The fiber number on the slides was counted under a polarized light microscope (PLM) (Olympus BX51N-31P-O PLM, Tokyo, Japan) (PLM detects all fibers longer than 200 nm). The results are shown in Fig. S1C.

Intrapulmonary spraying of MWCNT and CRO into the lung and pleural cavity lavage (PCL). We used the intrapulmonary spraying technique that was developed in our laboratory.[24] Briefly, rats were anaesthetized using isoflurane; the mouth was fully opened with the tongue gently held and the nozzle of a microsprayer (series IA-1B Intratracheal Aerosolizer; Penn-century, Philadelphia, PA, USA) was inserted into the trachea through the larynx and 0.5 mL suspension was sprayed into the lungs synchronizing with spontaneous respiratory inhalation. We confirmed that the dosed materials were distributed deep into the lung tissue and reached most of the terminal alveoli without causing obvious respiratory distress.

Ten-week-old male Fisher 344 rats were divided into four groups of six animals each and given 0.5 mL of saline containing 0.1% Tween 20 or 500 μg/mL MWCNT-N, MWCNT-M or CRO suspension by IPS once every other day five times over a 9-day period. The total amount of fibers administered was 1.25 mg/rat. Six hours after the last IPS, the rats were placed under deep isoflurane anesthesia; a small incision was made in the abdominal wall, the pleural cavity was injected with 10 mL of ice cold RPMI 1640 through the diaphragm, and the lavage fluid was collected by syringe. The rats were then killed by exsanguination from the inferior vena cava and the major organs, including the lung, chest wall, brain, liver, kidney, spleen and mediastinal lymph nodes, were fixed in 4% paraformaldehyde and processed for histological examination.

Analysis of inflammatory reaction in the pleural cavity. Cells in the lavage fluid were counted using a hemocytometer (Erma Co., Ltd, Tokyo, Japan), and the cellular fraction was then isolated by centrifugation at 200*g* for 5 min at 4°C. Cell pellets collected from three rats were combined (generating a total of two cell pellets per group), fixed in 4% paraformaldehyde and processed for histological examination. Total protein in the supernatants of each of the lavage fluids was determined using the Pierce BCA Protein Assay Kit (Thermo Scientific, Rockford, IL, USA) and the supernatants were then concentrated by centrifugation in Vivaspin 15 concentrators (Sartorius Stedium Biotech, Goettingen, Germany) at 1500*g* for 30 min at 4°C and used for *in vitro* cell proliferation assays.

Light microscopy and PLM. Haematoxylin–eosin (H&E)-stained slides of the lung tissues and cellular pellets of the PCL were used to observe MWCNT-N, MWCNT-M and CRO fibers with PLM at ×1000 magnification. The exact localization of the illuminated fibers was confirmed in the same H&E-stained sections after removing the polarizing filter.

Scanning electron microscopy. The H&E-stained slides of the lung tissue and PCL pellets were immersed in xylene for 3 days to remove the cover glass, then immersed in 100% ethanol for 10 min to remove the xylene and air-dried for 2 h at room temperature. The slides were then coated with platinum for viewing using a scanning electronic microscope (SEM) (Model S-4700 Field Emission SEM; Hitachi High Technologies Corporation, Tokyo, Japan) at 5–10 kV.

Immunohistochemistry and Azan–Mallory staining. CD68, proliferating cell nuclear antigen (PCNA) and mesothelin/Erc were detected using antirat CD68 antibodies (BMA Biomedicals, Augst, Switzerland), anti-PCNA monoclonal antibodies (Clone PC10; Dako Japan Inc., Tokyo, Japan) and antirat C-ERC/mesothelin polyclonal antibodies (Immuno-Biological Laboratories Co., Ltd, Gunma, Japan). The CD68, PCNA and C-ERC/mesothelin antibodies were diluted 1:100, 1:200 and 1:1000, respectively, in blocking solution and applied to deparaffinized slides. The slides were incubated at 4°C overnight and then incubated for 1 h with biotinylated species-specific secondary antibodies diluted 1:500 (Vector Laboratories, Burlingame, CA, USA) and visualized using avidin-conjugated horseradish peroxidase complex (ABC kit; Vector Laboratories). Azan–Mallory staining was used to visualize collagen fibers.

***In vitro* exposure and preparation of conditioned macrophage culture media.** The induction and preparation of primary alveolar macrophages (PAM) has been described previously.[24] PAM were seeded into 6 cm culture dishes at 2×10^6 cells per well in 10% FBS RPMI 1640. After overnight incubation, the culture media was refreshed and MWCNT-N, MWCNT-M or CRO suspensions were added to the cells to a final concentration of 10 μg/mL. The cells were then incubated for another 24 h. The conditioned macrophage culture media was then collected for *in vitro* cell proliferation assays.

***In vitro* cell proliferation assay.** Human mesothelioma cells, TCC-MESO1, derived from a patient in the Tochigi Cancer Center,[25] were seeded into 96-well culture plates at 2×10^3 cells per well in 10% FBS RPMI 1640. After overnight incubation, the cells were serum-starved for 24 h. The media was changed to 100 μL of the concentrated supernatants of the PCL or conditioned macrophage culture media and incubated for 72 h. The relative cell number was then determined using the Cell Counting Kit-8 (Dojindo Molecular Technologies, Rockville, MD, USA) according to the manufacturer's instruction.

Statistical analysis. Statistical analysis was performed using ANOVA. The statistical significance was analyzed using a two-tailed Student's *t*-test. A *P*-value of <0.05 was considered to be significant.

Results

Translocation of MWCNT and CRO fibers into the pleural cavity. The cell pellets of the PCL were used to examine whether

doi: 10.1111/cas.12005

the MWCNT or CRO fibers were present in the pleural cavity. We first screened the H&E-stained PCL cell pellet slides using PLM. The exact localization of the fibers was confirmed using SEM of the same slide sections. MWCNT-N, MWCNT-M and CRO fibers were present in PCL cell pellets, with most of the fibers in macrophage-like cells (Fig. 1a–c) with very few fibers located in the intercellular space or on cell surfaces (data not shown). Immunohistochemistry with CD68, a macrophage marker, showed that MWCNT and CRO fibers were mainly found in macrophages (Fig. 1d,e).

In tissue sections, MWCNT and CRO fibers were mainly detected in focal granulomatous lesions in the alveoli and in alveolar macrophages. Fibers were also found in the mediastinal lymph nodes, and a few fibers were detected in liver sinusoid cells, blood vessel wall cells in the brain, renal tubular cells and spleen sinus and macrophages (data not shown). We detected only a few fibers penetrating directly from the lung to the pleural cavity through the visceral pleura (Fig. S2) and did not find any fibers in the parietal pleura.

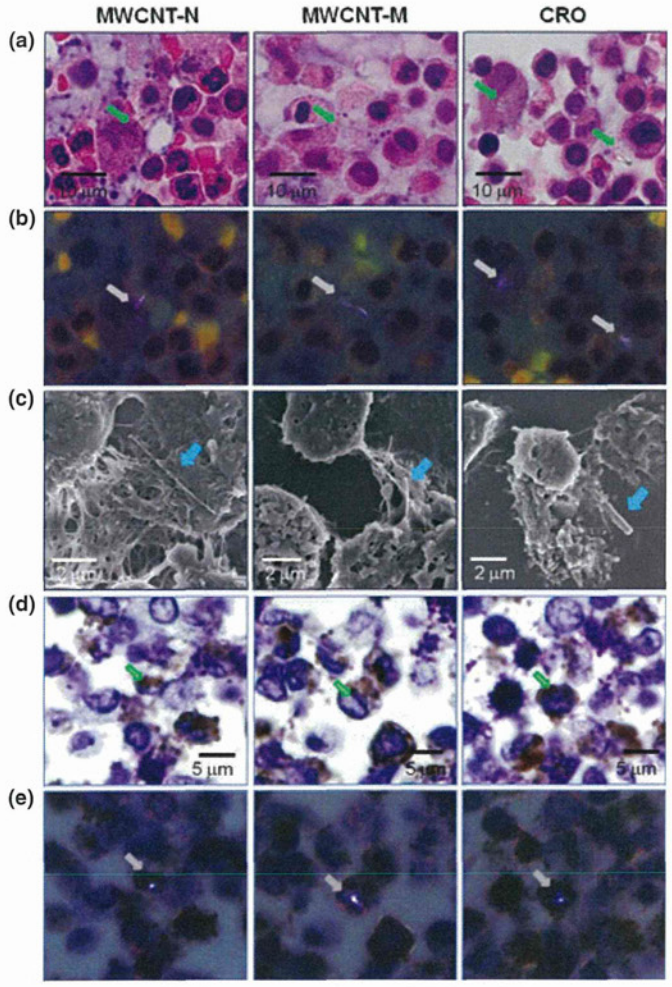

Fig. 1. Existence of multi-walled carbon nanotubes (MWCNT)-N, MWCNT-M and crocidolite (CRO) fibers in the cell pellets of the pleural cavity lavage (PCL). (a) Images of H&E-stained slides of the cell pellets of the PCL treated with MWCNT-N, MWCNT-M and CRO fibers. (b) Polarized light microscope (PLM) images of the same view areas shown in (a). (c) Scanning electron microscope observation showed the existence of the MWCNT and CRO fibers in the cell pellets of the PCL. (d) CD68 immunostaining of the PCL cell pellet slides. (e) PLM observation of the same view areas shown in (d) indicate that MWCNT and CRO fibers were present in the CD68-positive macrophages. Arrows indicate MWCNT-N, MWCNT-M and CRO fibers.

Induction of visceral mesothelial proliferation. Hyperplastic visceral mesothelial proliferation (HVMP) was clearly observed in all of the MWCNT and CRO treated groups. The HVMP lesions were composed of mesothelial cells with cuboidal appearance and increased size and density lining the visceral pleural tissue. Various degrees of lung inflammation and fibrous thickening were observed underneath the HVMP lesions (Fig. 2a, panel A). The PCNA immunostaining showed proliferating mesothelial cells within the HVMP lesions (Fig. 2a, panel B). The PCNA indices of the visceral mesothelium were increased approximately 10-fold in all the MWCNT and CRO treated groups compared with the control group

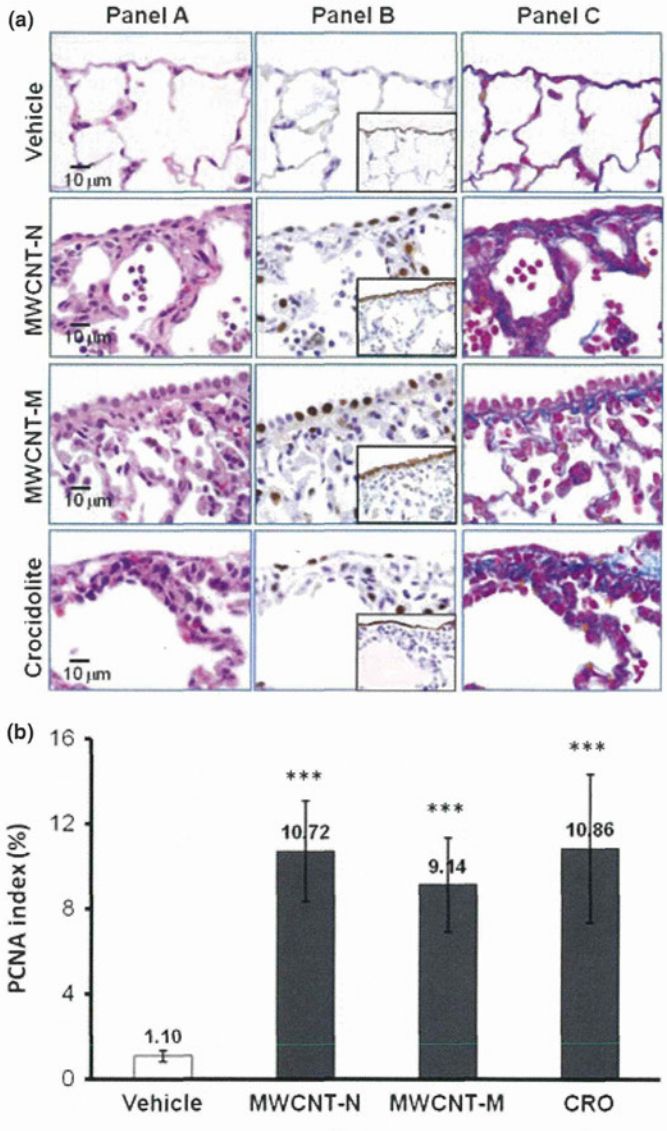

Fig. 2. Induction of visceral mesothelial cell proliferation lesions by treatment with multi-walled carbon nanotubes (MWCNT)-N, MWCNT-M or crocidolite (CRO). (a) Serial sections were prepared and stained with H&E, proliferating cell nuclear antigen (PCNA), Erc/mesothelin and Azan–Mallory's collagen staining. Panel A: increase in enlarged visceral mesothelial cells with cuboidal shapes in the MWCNT-N, MWCNT-M and CRO treated groups. Panel B: PCNA-positive cells are clearly increased in the dosed groups. The inserts are immunostained with Erc/mesothelin and show the lining of the mesothelium. Panel C: Azan–Mallory's staining; sub-pleural collagenous fibrosis is present under the mesothelial cell proliferation lesions. (b) PCNA index, expressed as the percentage of PCNA-positive cells of the total number of visceral mesothelial cells per slide. ***$P < 0.001$.

(Fig. 2b). Azan–Mallory staining showed increases in collagen fibers underneath the HVMP lesions (Fig. 2a, panel C). Fibers were not found within the HVMP lesions themselves. Alveolar macrophages with phagocytosed MWCNT or CRO fibers were frequently observed near the HVMP lesions (Fig. S3). Proliferation and other lesions of the parietal mesothelium were not observed.

Inflammatory cell infiltration in the pleural cavity. Both MWCNT and CRO treatment resulted in inflammatory reactions in the pleural cavity. The total number of cells, composed mostly of macrophages, neutrophils and lymphocytes, in the PCL in the MWCNT and CRO treated groups was significantly increased compared with the control group (Fig. 3a). As can be calculated from Fig. 3(a,b), macrophages accounted for a large part of the increase of the total cell number in the PCL, although the number of neutrophils and lymphocytes also increased. Overall, the proportion of macrophages in the cell pellets of the PCL was increased, while those of neutrophils and lymphocytes were decreased (Fig. 3b). MWCNT or CRO treatment also significantly increased the total protein level in the PLC (Fig. 3c). The proportion of cells in the PCL pellets positive for Mesothelin/Erc, a mesothelial cell marker, was 0.53–1.02%, and no intergroup difference was observed (data not shown). These data indicate that the increased cell number in the pleural cavity of the rats treated with MWCNT or CRO resulted from inflammatory cell effusion, not from mesothelial cell shedding of the pleural tissue. Many macrophages in the PCL contained MWCNT or CRO fibers.

Mesothelial cell proliferation assay *in vitro*. To examine whether inflammatory reactions, especially those mediated by macrophages, exert proliferative effects on mesothelial cells, we examined the effects of conditioned macrophage culture medium on mesothelial cell proliferation *in vitro*. The conditioned culture media of macrophages exposed to MWCNT-N, MWCNT-M or CRO significantly increased the proliferation of the human mesothelioma cell line TCC-MESO1. The concentrated supernatants of the PCL taken from the rats treated with MWCNT-N, MWCNT-M or CRO exhibited similar effects (Fig. 4). These results indicate that factors in the PCL, possibly secreted by alveolar and pleural macrophages, are able to cause mesothelial cell proliferation.

Discussion

In the present study, we compared the pleural translocation of MWCNT and CRO and examined the mesothelial lesions they induced. Our data demonstrate that after deposition in the lung, MWCNT, like CRO, translocated into the pleural cavity, mainly in pleural macrophages. Both MWCNT and CRO treatment also caused hyperplastic visceral mesothelial proliferation and marked pleural inflammation.

This is the first report to show that MWCNT administered into the rat lung causes mesothelial proliferative lesions. Adamson *et al.*[26] reported that intratracheal instillation of asbestos in mice induced pleural mesothelial cell proliferation within several days; the degree of pleural mesothelial cell proliferation did not appear to correlate with the localization of asbestos fibers in the pleura.[27] Similarly, we did not find fibers within the HVMP lesions. Thus, our findings suggest that HVMP lesions do not appear to be directly induced by the deposited MWCNT or CRO fibers. Also, *in vitro* exposure to MWCNT and CRO fibers did not lead to proliferation of TCC-MESO1 cells, but rather to cell death (Fig. S4). It has been reported that macrophages play a significant role in mesothelial cell proliferation caused by asbestos exposure and surgical injury,[28–31] and that the conditioned medium of macrophages

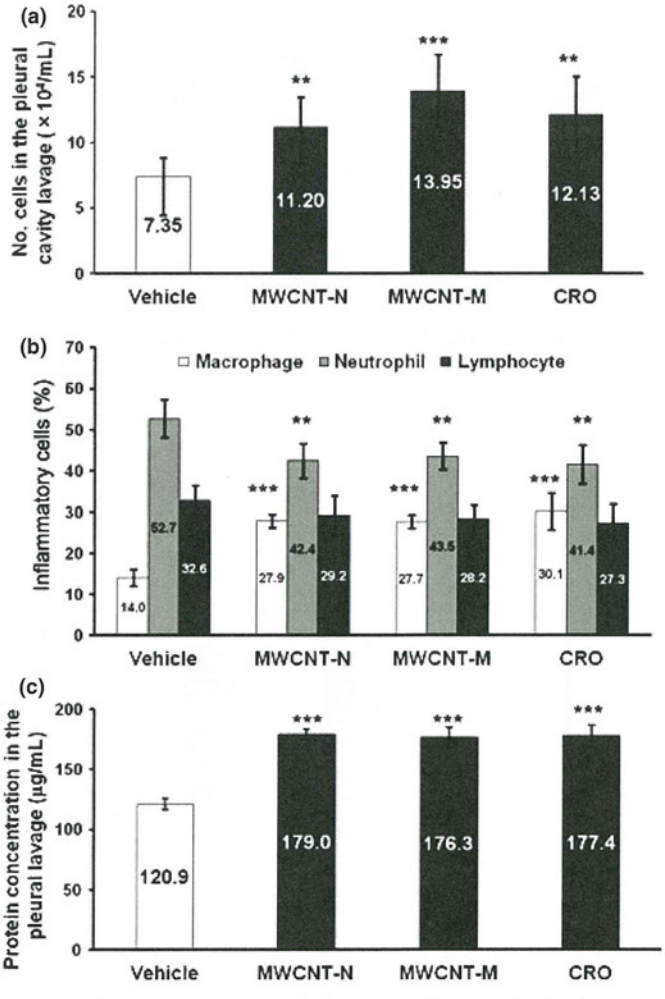

Fig. 3. Inflammatory reaction in the pleural cavity. (a) The number of leukocytes in the pleural cavity lavage (PCL) of rats treated with multi-walled carbon nanotubes (MWCNT) and crocidolite (CRO). (b) The proportion of macrophages, neutrophils and lymphocytes in the cell pellets of the PCL. Total cell number and cell numbers of macrophages, neutrophils and lymphocytes in 10 randomly chosen fields (×400) were counted. (c) Protein concentration in the supernatants of the PCL. $^{**}P < 0.01$; $^{***}P < 0.001$.

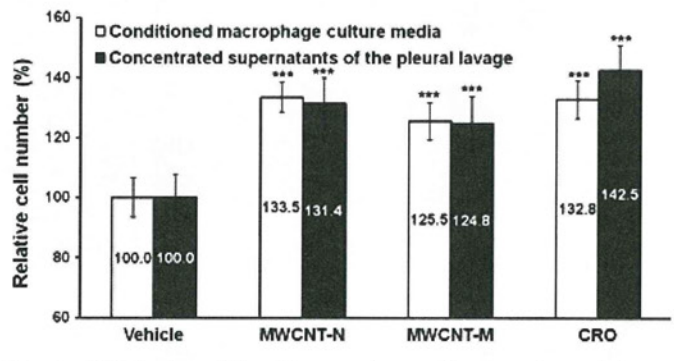

Fig. 4. Effect of conditioned macrophage culture media and the supernatants of the pleural cavity lavage (PCL) on mesothelial cell proliferation *in vitro*. The conditioned culture media of macrophages treated with multi-walled carbon nanotubes (MWCNT)-N, MWCNT-M or crocidolite (CRO) significantly increased the cell proliferation of TCC-MESO1. The concentrated supernatants of the PCL from the rats treated with MWCNT-N, MWCNT-M or CRO had similar effects. $n = 6$. $^{***}P < 0.001$.

doi: 10.1111/cas.12005

exposed to MWCNT promotes mesothelial cell proliferation *in vitro*.[30] Activated macrophages secrete a panel of growth factors and cytokines to regulate cell proliferation, which can augment transformation of mesothelial cells.[28,30,32,33] Our observations that mesothelial cell proliferation is enhanced by conditioned macrophage culture media and by the supernatants of pleural cavity lavage are consistent with these results, although the factors that are involved need to be identified.

Translocation of asbestos[34,35] and MWCNT[18] fibers from the lung to the pleural cavity has been found in rodents. This translocation also probably occurs in humans since asbestos fibers have been detected in human pleural lesions.[36] However, the mechanism and route of translocation are unclear. It has been suggested that penetration through the visceral pleura, possibly driven by increased pulmonary interstitial pressure and assisted by enhanced permeability of the visceral pleura due to asbestos-induced inflammation might be a major route.[37] In the present study, only a few MWCNT and CRO fibers were observed penetrating through the visceral pleura, and a large number of the fibers in the pleural cavity was observed in macrophages. We also observed frequent deposition of MWCNT and CRO in the mediastinal lymph nodes, mostly phagocytosed by macrophages. These results suggest that a probable route of translocation of the fibers is lymphatic flow. Inflammation in the pleural cavity is probably a defense response against translocated fibers. Murphy *et al.*[19] reported that intrapleural injection of 5 μg/mouse of long MWCNT or asbestos initiated sustained inflammation, including increased granulocyte number and protein level, in the pleural cavity. Thus, the observed proliferation of visceral mesothelial cells in the present study is probably caused by inflammatory reactions both in the lung and in the pleural cavity. In the present study, no MWCNT or crosidolite fibers or lesions were observed in the parietal pleura. This is possibly due to the short experimental period and limited amount of fibers in the pleural cavity, which would result in little inflammation in the parietal pleura.

Currently, the exposure level to MWCNT in the workplace is unknown and there are no administrational regulations for the occupational exposure limit for MWCNT. In November 2010, the National Institute of Occupational Safety and Health (NIOSH) released a non-official carbon nanotube exposure limit for peer review. The recommended exposure limit in the air was set at 7 $\mu g/m^3$.[38] Previously, we used a total dose of 1.25 mg/rat of titanium dioxide over a 9-day period and identified factors involved in titanium dioxide-induced lung lesions.[24] In the present study, we used the same protocol for the purpose of induction of observable pleural lesions and inflammation in the pleural cavity as well to ensure the presence of a detectable number of fibers in the pleural cavity after short-term administration; this dose was higher than the NIOSH exposure limit. Time- and dose-dependent experiments are needed in future studies, and further investigation is also required to elucidate cytokines and other factors that cause parietal mesothelial proliferation in animal models that are more relevant to humans.

The IPS/intratracheal instillation is a widely used method to evaluate the respiratory toxicity of particles. It should be noted that IPS/intratracheal instillation is a non-physiological method and possibly affects the migration and distribution of particles in the lung due to the pressure from spraying. However, IPS/intratracheal instillation is relevant for identifying factors to be examined using long-term, more physiologically relevant methods of CNT administration.

In summary, MWCNT and CRO fibers were found to translocate from the lung to the pleural cavity after intrapulmonary administration. Importantly, MWCNT and CRO treatment caused visceral mesothelial cell proliferation and inflammation in the pleural cavity. This mesothelial proliferation was plausibly induced by inflammatory events in the lung and pleural cavity and mediated primarily by macrophages. The similarity between MWCNT-N, MWCNT-M and CRO in translocation to the pleural cavity, induction of pleural cavity inflammation and induction of visceral pleural mesothelial proliferation suggests that MWCNT might cause asbestos-like pleural lesions.

Acknowledgments

This work was supported by Health and Labour Sciences Research Grants (Research on Risk of Chemical Substance 21340601) (grant numbers H19-kagaku-ippan-006, H22-kagaku-ippan-005).

Disclosure Statement

The authors have no conflict of interest.

References

1 Bonner JC. Nanoparticles as a potential cause of pleural and interstitial lung disease. *Proc Am Thorac Soc* 2010; **7**: 138–41.
2 Donaldson K, Murphy FA, Duffin R *et al.* Asbestos, carbon nanotubes and the pleural mesothelium: a review of the hypothesis regarding the role of long fibre retention in the parietal pleura, inflammation and mesothelioma. *Part Fibre Toxicol* 2010; **7**: 5.
3 Johnston HJ, Hutchison GR, Christensen FM *et al.* A critical review of the biological mechanisms underlying the *in vivo* and *in vitro* toxicity of carbon nanotubes: the contribution of physico-chemical characteristics. *Nanotoxicology* 2010; **4**: 207–46.
4 Nagai H, Toyokuni S. Biopersistent fiber-induced inflammation and carcinogenesis: lessons learned from asbestos toward safety of fibrous nanomaterials. *Arch Biochem Biophys* 2010; **502**: 1–7.
5 Pacurari M, Castranova V, Vallyathan V. Single- and multi-wall carbon nanotubes versus asbestos: are the carbon nanotubes a new health risk to humans? *J Toxicol Environ Health A* 2010; **73**: 378–95.
6 Tsuda H, Xu J, Sakai Y *et al.* Toxicology of engineered nanomaterials – a review of carcinogenic potential. *Asian Pac J Cancer Prev* 2009; **10**: 975–80.
7 Barrett JC. Cellular and molecular mechanisms of asbestos carcinogenicity: implications for biopersistence. *Environ Health Perspect* 1994; **102** (Suppl 5): 19–23.
8 Miller BG, Searl A, Davis JM *et al.* Influence of fibre length, dissolution and biopersistence on the production of mesothelioma in the rat peritoneal cavity. *Ann Occup Hyg* 1999; **43**: 155–66.
9 Okada F. Beyond foreign-body-induced carcinogenesis: impact of reactive oxygen species derived from inflammatory cells in tumorigenic conversion and tumor progression. *Int J Cancer* 2007; **121**: 2364–72.
10 Stanton MF, Wrench C. Mechanisms of mesothelioma induction with asbestos and fibrous glass. *J Natl Cancer Inst* 1972; **48**: 797–821.
11 Walker C, Everitt J, Barrett JC. Possible cellular and molecular mechanisms for asbestos carcinogenicity. *Am J Ind Med* 1992; **21**: 253–73.
12 Yang H, Testa JR, Carbone M. Mesothelioma epidemiology, carcinogenesis, and pathogenesis. *Curr Treat Options Oncol* 2008; **9**: 147–57.
13 Poland CA, Duffin R, Kinloch I *et al.* Carbon nanotubes introduced into the abdominal cavity of mice show asbestos-like pathogenicity in a pilot study. *Nat Nanotechnol* 2008; **3**: 423–8.
14 Sakamoto Y, Nakae D, Fukumori N *et al.* Induction of mesothelioma by a single intrascrotal administration of multi-wall carbon nanotube in intact male Fischer 344 rats. *J Toxicol Sci* 2009; **34**: 65–76.
15 Takagi A, Hirose A, Nishimura T *et al.* Induction of mesothelioma in p53+/– mouse by intraperitoneal application of multi-wall carbon nanotube. *J Toxicol Sci* 2008; **33**: 105–16.
16 Takagi A, Hirose A, Futakuchi M *et al.* Dose-dependent mesothelioma induction by intraperitoneal administration of multi-wall carbon nanotubes in p53 heterozygous mice. *Cancer Sci* 2012; **103**: 1440–4.
17 Ryman-Rasmussen JP, Cesta MF, Brody AR *et al.* Inhaled carbon nanotubes reach the subpleural tissue in mice. *Nat Nanotechnol* 2009; **4**: 747–51.
18 Mercer RR, Hubbs AF, Scabilloni JF *et al.* Distribution and persistence of pleural penetrations by multi-walled carbon nanotubes. *Part Fibre Toxicol* 2010; **7**: 28.

19 Murphy FA, Poland CA, Duffin R *et al.* Length-dependent retention of carbon nanotubes in the pleural space of mice initiates sustained inflammation and progressive fibrosis on the parietal pleura. *Am J Pathol* 2011; **178**: 2587–600.
20 Oka Y, Mitsui M, Kitahashi T *et al.* A reliable method for intratracheal instillation of materials to the entire lung in rats. *J Toxicol Pathol* 2006; **19**: 107–9.
21 Jackson P, Hougaard KS, Boisen AM *et al.* Pulmonary exposure to carbon black by inhalation or instillation in pregnant mice: effects on liver DNA strand breaks in dams and offspring. *Nanotoxicology* 2012; **6**: 486–500.
22 Morimoto Y, Hirohashi M, Ogami A *et al.* Pulmonary toxicity of well-dispersed multi-wall carbon nanotubes following inhalation and intratracheal instillation. *Nanotoxicology* 2012; **6**: 587–99.
23 Ogami A, Yamamoto K, Morimoto Y *et al.* Pathological features of rat lung following inhalation and intratracheal instillation of C(60) fullerene. *Inhal Toxicol* 2011; **23**: 407–16.
24 Xu J, Futakuchi M, Iigo M *et al.* Involvement of macrophage inflammatory protein 1alpha (MIP1alpha) in promotion of rat lung and mammary carcinogenic activity of nanoscale titanium dioxide particles administered by intrapulmonary spraying. *Carcinogenesis* 2010; **31**: 927–35.
25 Yanagihara K, Tsumuraya M, Takigahira M *et al.* An orthotopic implantation mouse model of human malignant pleural mesothelioma for *in vivo* photon counting analysis and evaluation of the effect of S-1 therapy. *Int J Cancer* 2010; **126**: 2835–46.
26 Adamson IY, Bakowska J, Bowden DH. Mesothelial cell proliferation after instillation of long or short asbestos fibers into mouse lung. *Am J Pathol* 1993; **142**: 1209–16.
27 Sekhon H, Wright J, Churg A. Effects of cigarette smoke and asbestos on airway, vascular and mesothelial cell proliferation. *Int J Exp Pathol* 1995; **76**: 411–8.
28 Adamson IY, Prieditis H, Young L. Lung mesothelial cell and fibroblast responses to pleural and alveolar macrophage supernatants and to lavage fluids from crocidolite-exposed rats. *Am J Respir Cell Mol Biol* 1997; **16**: 650–6.
29 Li XY, Lamb D, Donaldson K. Mesothelial cell injury caused by pleural leukocytes from rats treated with intratracheal instillation of crocidolite asbestos or *Corynebacterium parvum*. *Environ Res* 1994; **64**: 181–91.
30 Murphy FA, Schinwald A, Poland CA *et al.* The mechanism of pleural inflammation by long carbon nanotubes: interaction of long fibres with macrophages stimulates them to amplify pro-inflammatory responses in mesothelial cells. *Part Fibre Toxicol* 2012; **9**: 8.
31 Mutsaers SE, Whitaker D, Papadimitriou JM. Stimulation of mesothelial cell proliferation by exudate macrophages enhances serosal wound healing in a murine model. *Am J Pathol* 2002; **160**: 681–92.
32 Lechner JF, LaVeck MA, Gerwin BI *et al.* Differential responses to growth factors by normal human mesothelial cultures from individual donors. *J Cell Physiol* 1989; **139**: 295–300.
33 Wang Y, Faux SP, Hallden G *et al.* Interleukin-1beta and tumour necrosis factor-alpha promote the transformation of human immortalised mesothelial cells by erionite. *Int J Oncol* 2004; **25**: 173–8.
34 Choe N, Tanaka S, Xia W *et al.* Pleural macrophage recruitment and activation in asbestos-induced pleural injury. *Environ Health Perspect* 1997; **105** (Suppl 5): 1257–60.
35 Viallat JR, Raybuad F, Passarel M *et al.* Pleural migration of chrysotile fibers after intratracheal injection in rats. *Arch Environ Health* 1986; **41**: 282–6.
36 Kohyama N, Suzuki Y. Analysis of asbestos fibers in lung parenchyma, pleural plaques, and mesothelioma tissues of North American insulation workers. *Ann N Y Acad Sci* 1991; **643**: 27–52.
37 Miserocchi G, Sancini G, Mantegazza F *et al.* Translocation pathways for inhaled asbestos fibers. *Environ Health* 2008; **7**: 4.
38 NIOSH. Occupational exposure to carbon nanotubes and nanofibers. *Curr Intelligence Bull* 2010; **161-A**: 1–149.

Supporting Information

Additional Supporting Information may be found in the online version of this article:

Fig. S1. Characterization of multi-walled carbon nanotubes and crocidolite fibers in the suspensions.
Fig. S2. SEM observation of multi-walled carbon nanotubes and crocidolite fibers in the visceral pleura.
Fig. S3. Inflammation and fibrosis in the lung.
Fig. S4. Cytotoxicity of multi-walled carbon nanotubes and crocidolite to TCC-MESO1 cells *in vitro*.

doi: 10.1111/cas.12005

J Toxicol Pathol 2012; 25: 233–239

Original Article

Acute Phase Pulmonary Responses to a Single Intratracheal Spray Instillation of Magnetite (Fe_3O_4) Nanoparticles in Fischer 344 Rats

Yukie Tada[1*], Norio Yano[1], Hiroshi Takahashi[1], Katsuhiro Yuzawa[1], Hiroshi Ando[1], Yoshikazu Kubo[1], Akemichi Nagasawa[1], Akio Ogata[1], and Dai Nakae[1,2*]

[1] Departments of Environmental Health and Toxicology, Tokyo Metropolitan Institute of Public Health, 3-24-1 Hyakunin-cho, Shinjuku-ku, Tokyo 169-0073, Japan
[2] Tokyo University of Agriculture, 1-1-1 Sakuragaoka, Setagaya-ku, Tokyo 156-8502, Japan

Abstract: Iron nanomaterials are of considerable interest for application to nanotechnology-related fields including environmental catalysis, biomedical imaging, drug delivery and hyperthermia, because of their superparamagnetic characteristics and high catalytic abilities. However, information about potential risks of iron nanomaterials is limited. The present study assessed pulmonary responses to a single intratracheal spray instillation of triiron tetraoxide nanoparticles (magnetite) in rats. Ten-week-old male and female Fischer 344 rats (n=5/group) were exposed to a single intratracheal spray instillation of 0 (vehicle), 5.0, 15.0 or 45.0 mg/kg body weight (BW) of magnetite. After 14 days, the rats were sacrificed, and biological consequences were investigated. The lung weights of the 15.0 and 45.0 mg/kg BW male and female groups were significantly higher than those of the control groups. The lungs of treated rats showed enlargement and black patches originating from the color of magnetite. The typical histopathological changes in the lungs of the treated rats included infiltration of macrophages phagocytosing magnetite, inflammatory cell infiltration, granuloma formation and an increase of goblet cells in the bronchial epithelium. The results clearly show that instilled magnetite causes foreign body inflammatory and granulating lesions in the lung. These pulmonary responses occur in a dose-dependent manner in association with the increase in lung weight. (DOI: 10.1293/tox.25.233; J Toxicol Pathol 2012; 25: 233–239)

Key words: magnetite, Fe_3O_4, nanoparticles, lung, intratracheal spray instillation, Fischer 344 rat

Introduction

Nanomaterials are defined as having a size of 100 nanometers or less in at least one dimension. Nanotechnology -the creation, manipulation and application of nanomaterials- involves the ability to engineer, control and exploit the unique chemical, physical and electrical properties that emerge from infinitesimally tiny man-made particles[1]. Engineered nanoparticles, the surface volume increases, can result in having unique photonic and catalytic properties that display great differences from those of over-nanoscaled materials with the same composition. The superb biological and environmental reactivities of nanoparticles have led to their wide and considerable use in disease treatment, pollutant degradation and so forth[1, 2]. Among them, iron nanomaterials are of considerable interest for application to nanotechnology-related fields including environmental catalysis, magnetic storage, biomedical imaging[1], magnetic target drug delivery[3, 4] and hyperthermia[5–8] because of their superparamagnetic characteristics and high catalytic abilities.

Acute toxic reactions of nano-magnetic ferrofluid have been evaluated, and half lethal doses (LD_{50}) of >2104.8, >438.50 and >1578.6 mg/kg were found in cases of oral, intravenous and intraperitoneal administrations, respectively, where no apparent pathological changes were observed[9]. It was shown *in vitro* that triiron tetraoxide, Fe_3O_4, causes a decrease in mitochondrial function and lactate dehydrogenase leakage in Neuro-2A cells only with concentrations reaching greater than 200 μg/mL[10]. Magnetic nanoparticles of Fe_3O_4 affect the ICR mice immune system such that Fe_3O_4 nanoparticles enhance the production of interleukin (IL)-2, interferon-γ and IL-10, but not IL-4, in the peripheral blood[11]. A high amount of magnetite, 15 mg × 15 intratracheal instillations, led to an unexpected lung tumor in the female Wistar rat[12], while chronic exposure to iron oxide has been shown not to increase the incidence of pulmonary tumors[13, 14]. Iron is a transition metal that is considered to play a pivotal role in modulating oxidative stress and other biological responses[15, 16], which is speculated to be the critical mechanism in eliciting the adverse effects of iron

Received: 12 March 2012 , Accepted: 19 June 2012
*Corresponding authors: Y Tada (e-mail: Yukie_Tada@member.metro.tokyo.jp), D Nakae (e-mail: agalennde.dai@nifty.com)

particulate matter exposure. Despite the above information, the risk data for iron nanomaterials are limited. The present study assessed pulmonary responses to a single intratracheal spray instillation of Fe_3O_4 nanoparticles (magnetite) in male and female Fischer 344 rats.

Materials and Methods

Ethical considerations

The current study was performed principally in conformity with the Guidelines for the Toxicity Testing of Pharmaceuticals released by the MHLW (Ministry of Health, Labour and Welfare) of Japan (http://www.pmda.go.jp/ich/s/s4_93_8_10.pdf). The experimental protocol was approved by the Experiments Regulation Committee and Animal Experiment Committee of the Tokyo Metropolitan Institute of Public Health prior to its execution. All the animals were handled in accordance with the Japanese Government Animal Protection and Management Law, Japanese Government Notification on Feeding and Safekeeping of Animals and the Guidelines for Animal Experimentation issued by the Japanese Association for Laboratory Animal Science[17].

Animals

A total of 42 male and female specific pathogen-free Fischer 344 (F344/DuCrlCrlj) rats were purchased at 8 weeks of age from Charles River Laboratories Japan, Inc. (Kanagawa, Japan). The rats were housed individually in stainless steel cages and were kept under controlled conditions of temperature (22–24°C), relative humidity (50–60%) and ventilation (more than 10 times/hour) with a 12-hour light/dark cycle; they were allowed free access to pelleted chow CE-2 (CLEA Japan, Inc., Tokyo, Japan) and drinking water throughout both the acclimation and experimental periods. After confirming normal health status at the end of the 2-week acclimation period, 20 rats of each sex were selected for use and randomly allocated to 4 groups of 5 rats. The rats were observed twice daily, and clinical signs and mortality were recorded.

Test chemical and animal treatments

The magnetite slurry (Fe_3O_4 nanoparticle suspension; lot number, 90828) was generously supplied by Toda Kogyo Corp. (Otake, Hiroshima, Japan). A representative transmission electron microscopic (TEM) view of magnetite particles is shown in Fig. 1. The estimated primary particle size of the prepared sample is 5–15 nm in diameter (TEM measurement). The purity of the test chemical was determined by an energy dispersive X-ray spectrometer, and only iron and oxygen were detected. Prior to the toxicity study, the optimal way to disperse magnetite was preliminarily examined. Magnetite was dispersed in physiological saline, physiological saline+0.05% tween 80, 0.1 M Tris buffer (pH 8.0), 0.5% carboxymethyl cellulose, 0.1 M phosphate buffer (pH 8.1) or ultrapure water (Milli-Q water, 18.2 MΩ). Observation of dispersed particles was carried out under a light microscope and judged on the basis of Brownian motion. Among

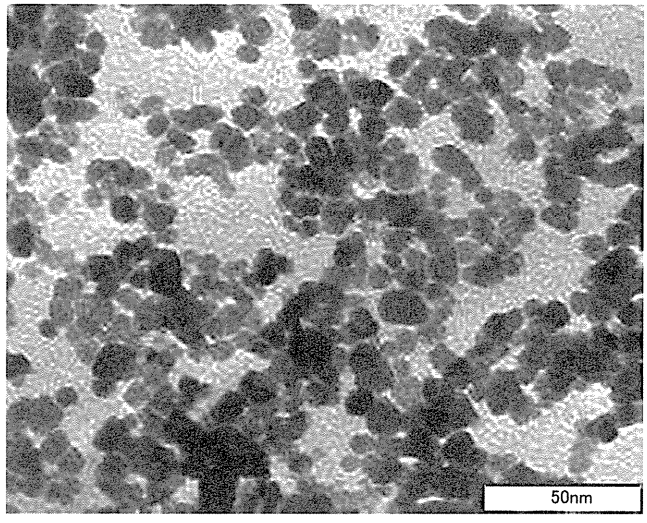

Fig. 1. Representative transmission electron microscopic view of magnetite nanoparticles. The estimated primary particle size is about 5–15 nm in diameter.

these test dispersion vehicles, Milli-Q water was the best vehicle to obtain the most homogeneous suspension. Magnetite slurry was thus diluted with sterile Milli-Q water and adjusted to about pH 7.4 with 0.1 N hydrochloric acid. The intratracheal instillation technique was performed according to the recommendations of Driscoll *et al.*[18]. Before the intratracheal spray instillation, the rats were anesthetized by diethyl ether and placed in a supine position on an angled board with their necks extended. Magnetite suspension was placed in an ultrasonication bath (SONOREX RK31, BANDELIN electronic, Berlin, Germany) and then instilled into the trachea by a sterile stainless steel tube (IA-1B Micro-Sprayer, Penn-Century, Inc., Wyndmoor, PA, USA) at the concentrations of 0 (control), 5.0 (low), 15.0 (middle) and 45.0 (high) mg/1 mL/kg body weight, which was followed by the insufflation of 0.2 mL of air.

Animal sacrifice and assessments

Two weeks after instillation, all rats were deprived of food (but not water) overnight. The rats were then lightly anesthetized by diethyl ether and sacrificed by exsanguination after collecting blood samples via the abdominal aorta. The blood for hematology was collected into tubes treated with dipotassium ethylenediaminetetraacetate (EDTA-2K). The hematological examination was carried out using an automatic analyzer (Sysmex KX-21NV; Sysmex Corporation, Kobe, Hyogo, Japan) to determine the red blood cell count (RBC), hemoglobin concentration (HGB), hematocrit level (HCT), mean corpuscular volume (MCV), mean corpuscular hemoglobin (MCH), mean corpuscular hemoglobin concentration (MCHC), white blood cell count (WBC) and platelet count (PLT). Differential counts of leukocytes were made by a light microscopic observation of smeared specimens stained with a routine May-Grünwald-Giemsa protocol. A serum biochemistry analysis was performed with an automatic analyzer (TBA-120FR; Toshiba Medical Systems

Table 1. Initial and Final Body Weights and Lung Weights in Fischer 344 Rats Treated with a Single Intratracheal Administration of Magnetite on Day 14

Item	Dose of magnetite (mg/kg body weight)			
	0 (control)	5.0	15.0	45.0
Males				
Initial number of rats	5	5	5	5
Initial body weight (g)	213.6 ± 3.9[a]	211.7 ± 5.5	214.9 ± 4.6	212.9 ± 4.0
Final effective number of rats	5	5	5	5
Final body weight (g)	239.4 ± 8.6	239.1 ± 7.4	239.1 ± 10.3	229.0 ± 2.8
Absolute lung weight (mg)	722.4 ± 27.4	823.8 ± 58.0	923.4 ± 91.5*	1105.1 ± 94.5*
Relative lung weight (mg/100 g BW)	301.9 ± 9.5	344.4 ± 19.4	386.4 ± 38.1*	482.5 ± 41.0*
Females				
Number of rats	5	5	5	5
Initial body weight (g)	138.9 ± 7.1	138.0 ± 5.8	138.6 ± 7.7	141.8 ± 9.3
Final effective number of rats	5	5	4	4
Final body weight (g)	151.0 ± 6.7	148.7 ± 6.1	149.3 ± 6.6	145.2 ± 12.4
Absolute lung weight (mg)	556.7 ± 77.2	642.1 ± 55.5	724.9 ± 88.1*	821.7 ± 68.0*
Relative lung weight (mg/100 g BW)	368.3 ± 46.6	431.3 ± 23.5	485.6 ± 57.7*	566.7 ± 32.6*

[a] Values are means ± standard deviations. *Significantly different from the corresponding control values ($P<0.05$, Dunnet's test).

Corporation, Tokyo, Japan) to determine the levels of total protein (TP), albumin (ALB), albumin/globulin ratio (A/G), glucose (GLU), aspartate aminotransferase (AST), alanine aminotransferase (ALT), total cholesterol (T-CHO), triglyceride (TG), total bilirubin (T-BIL), blood urea nitrogen (BUN), creatinine (CRE) and uric acid (UA). Upon sacrifice, the rats were macroscopically examined and subjected to a full autopsy. The brain, heart, lung (including bronchi, fixed by inflation with fixative), spleen, liver, kidneys, testes and ovaries were weighed and then fixed in 10% neutrally buffered formalin. Paraffin-embedded sections were routinely prepared and histopathologically examined after being stained with hematoxylin and eosin (HE), Azan Mallory and Berlin blue procedures.

Statistical analysis

For numerical data such as body and organ weights and hematological and serological outcomes, equality of means between the values of the control group and those of each treated group was assessed by Bartlett's test. Homogeneity of variance was then analyzed by one-way analysis of variance, and finally, differences between the values of the control group and those of each treated group were evaluated by Dunnett's test. If the Bartlett's test was significant, the data were subjected to the Kruskal-Wallis test and Dunnett's-type rank sum test. For contingent data such as incidences of histopathological lesions, differences between the values of the control group and those of each treated group were evaluated by Fisher's exact probability test[19]. Statistical processing was conducted using the StatLight software (Yukms Co., Ltd., Tokyo, Japan). Intergroup differences were considered statistically significant when P-values less than 0.05 were obtained.

Results

General findings

All male rats survived throughout the experimental period. In the females, one rat in each of the middle- and high-dose groups died within 1 hour from deep anesthesia following intratracheal spray instillation. After instillation, the male and female rats in the high-dose group were slightly less active than the control rats but recovered later.

Hematology and serum biochemistry

In the hematology, the HGB of the high-dose group males was significantly but slightly higher than that of the male control group. In the serum biochemistry, the A/G of the high-dose group females was significantly lower than that of the female control group. There were no significant differences in other items of hematology or biochemistry between the control and treated rats at any doses. Morphological findings and differential counts of leukocytes showed no significant effects in any of the treated groups.

Pathology

There were no significant differences in the initial or final body weights between the control and treated groups of either sex. Absolute and relative lung weights of the treated groups were higher than those of the control groups, and the differences were statistically significant for the middle- and high-dose groups (Table 1). In the male rats, the absolute and relative testes weights of the low-dose group were significantly higher than those of the control group. There were no significant differences in other organ weights between the control and treated groups for both sexes.

At necropsy, the lungs of the magnetite-treated groups of both sexes were enlarged, and scattered dark brown patches were observed in almost every lobe in all treated rats (Fig. 2). These changes were more marked in the middle- and high-dose groups than in the low-dose groups.

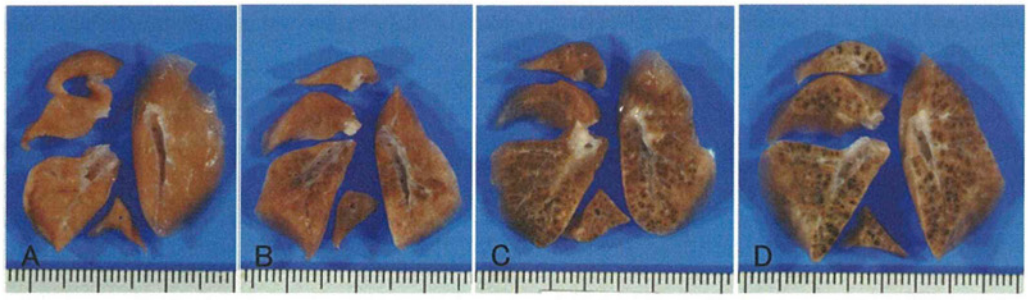

Fig. 2. Representative gross views of cross-sections of the formalin-fixed lungs from Fischer 344 rats treated with a single intratracheal spray instillation dose of 0 (control, A), 5.0 (B), 15.0 (C) or 45.0 (D) mg/kg body weight of magnetite on day 14. The enlargement and a large number of scattered dark brown patches are marked in almost every lobe at the middle and high doses.

Table 2. Histological Findings of the Lungs and Parathymic Lymph Nodes in Fischer 344 Rats Treated with a Single Intratracheal Administration of Magnetite on Day 14

Item	Dose of magnetite (mg/kg body weight)			
	0 (control)	5.0	15.0	45.0
Males				
Effective number of rats	5	5	5	5
Lung				
Inflammatory cell infiltration	0[a]	4*	4*	5*
Infiltration of macrophages phagocytosing magnetite	0	5*	5*	5*
Granuloma	0	1	3	5*
Increase of goblet cells in the bronchial epithelium	0	0	0	5*
Parathymic lymph nodes				
Infiltration of macrophages phagocytosing magnetite	0	5*	5*	5*
Deposit of magnetite	0	5*	5*	5*
Females				
Effective number of rats	5	5	4	4
Lung				
Inflammatory cell infiltration	0	3	4*	4*
Infiltration of macrophages phagocytosing magnetite	0	5*	4*	4*
Granuloma	0	0	1	4*
Increase of goblet cells in the bronchial epithelium	0	0	0	3
Parathymic lymph nodes				
Infiltration of macrophages phagocytosing magnetite	0	5*	4*	4*
Deposit of magnetite	0	5*	4*	4*

[a] Number of rats with the lesion. *Significantly different from the corresponding control values ($P<0.05$, Fisher's exact test). No apparent histological changes were observed in the other organs, when compared with the control rats.

Additionally, dark brown patches were also observed in the parathymic lymph nodes of male and female rats in all treated groups.

The histopathological changes in the lungs and parathymic lymph nodes are summarized in Table 2. In the lungs of most of the rats in all the treated groups, typically observed changes included the infiltration of multinucleated cells and lymphocytes (Fig. 3A) and the infiltration of dark-brownishly pigmented macrophages phagocytosing magnetite in the alveolar walls and spaces (Fig. 3B). In addition, granulomas were observed in 1, 3 and 5 of the low-, middle- and high-dose males and in 1 and 4 of the middle- and high-dose females, respectively. The granulomas were characterized by the aggregation of macrophages phagocytosing magnetite, inflammatory cell infiltration and proliferation of collagenous fiber (Fig. 3C and D). Reactive changes in alveolar and bronchial epithelia were observed in most of the rats of all treated groups and in the high-dose groups, respectively. An increase of goblet cells in the bronchial epithelium was observed in 5 and 3 of the high-dose males and females, respectively (Fig. 4). In the parathymic lymph nodes, infiltration of macrophages phagocytosing magnetite and deposits of magnetite particles were observed in male and female rats of all treated groups (Fig. 5). Dark-brownishly pigmented macrophages were observed at the center or end of the lymph node. No treatment-related changes were observed in other organs of either sex, whereas sporadic spontaneous lesions were observed identically in the control and treated rats.

Discussion

In the present study, rats were exposed to the magnetite nanoparticles by a single intratracheal spray instillation

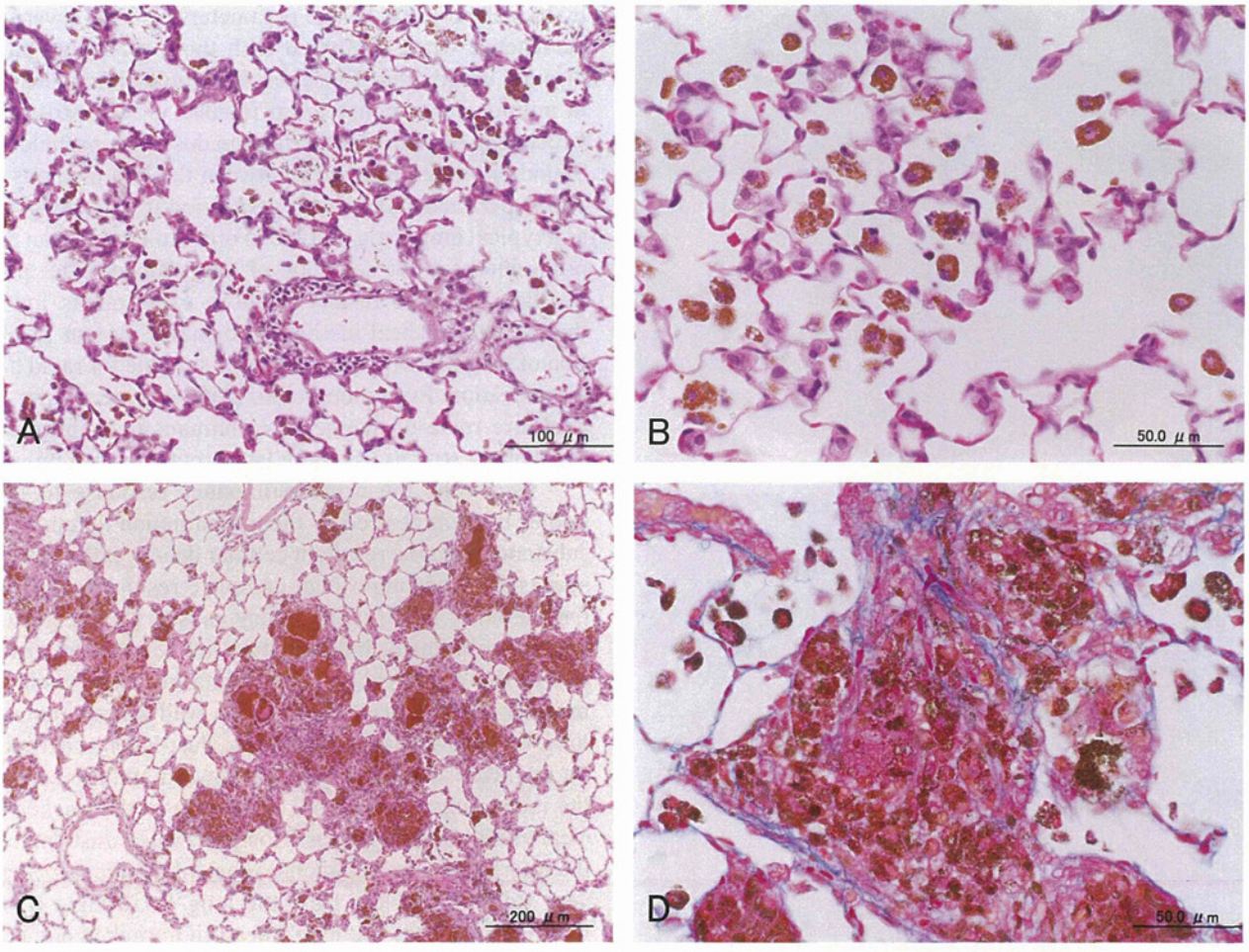

Fig. 3. Representative histologies of the lungs from Fischer 344 rats treated with a single intratracheal spray instillation dose of 5.0 (A, B) or 45.0 (C, D) mg/kg body weight of magnetite on day 14 (A–C, hematoxylin and eosin; D, Azan-Mallory). Infiltration of inflammatory cells (A) and alveolar macrophages phagocytosing magnetite particles (B) are evident in rats given the low dose. Granulomas consisting of macrophages with magnetite particles, infiltrating inflammatory cells and proliferative collagenous fiber (C and D) are evident in rats given the high dose.

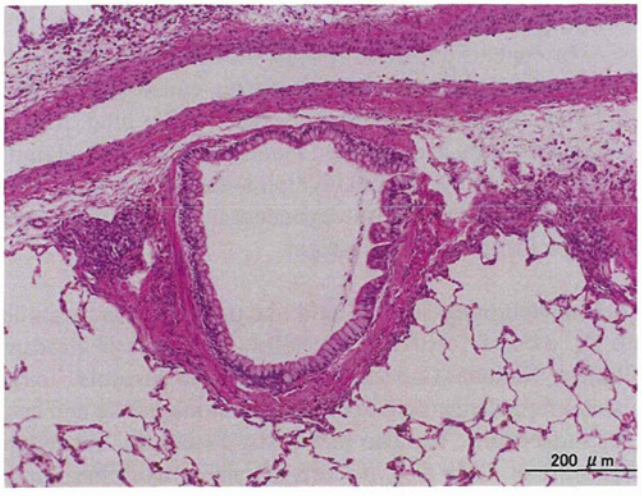

Fig. 4. Representative histology of the lung from Fischer 344 rat treated with a single intratracheal spray instillation dose of 45.0 mg/kg body weight of magnetite on day 14 (hematoxylin and eosin). An increase in goblet cells in the bronchial epithelium is evident in a rat given the high dose.

at the doses of 0, 5.0, 15.0 and 45.0 mg/kg body weight. Macroscopically, enlargement of the lung was marked at middle and high doses. Black patches were scattered in almost every lobe of the lungs and the lung-associated lymph nodes of all treated rats. Two weeks after instillation, a large amount of the administered magnetite remained in the lung, and some of the magnetite was distributed into the regional lymph nodes. Histopathologically, infiltration of macrophages phagocytosing magnetite, multinucleated cells and lymphocytes were observed in the lungs of the treated rats. In addition, granulomas were observed in the lungs of the treated rats. Infiltration of multinucleated cells and lymphocytes which supposed to be macrophages, generally indicates chronic change. From the present result, it was not clear whether the macrophages died because of frustrated phagocytosis.

In an inhalation (nose-only) toxicity test using pigment-sized Fe_3O_4 for Wistar rats, subchronic responses have been reported. Pulmonary inflammation was evidenced by bronchoalveolar lavage (BAL) fluid analysis, histopathology, particle deposition and increased lung and lung-asso-

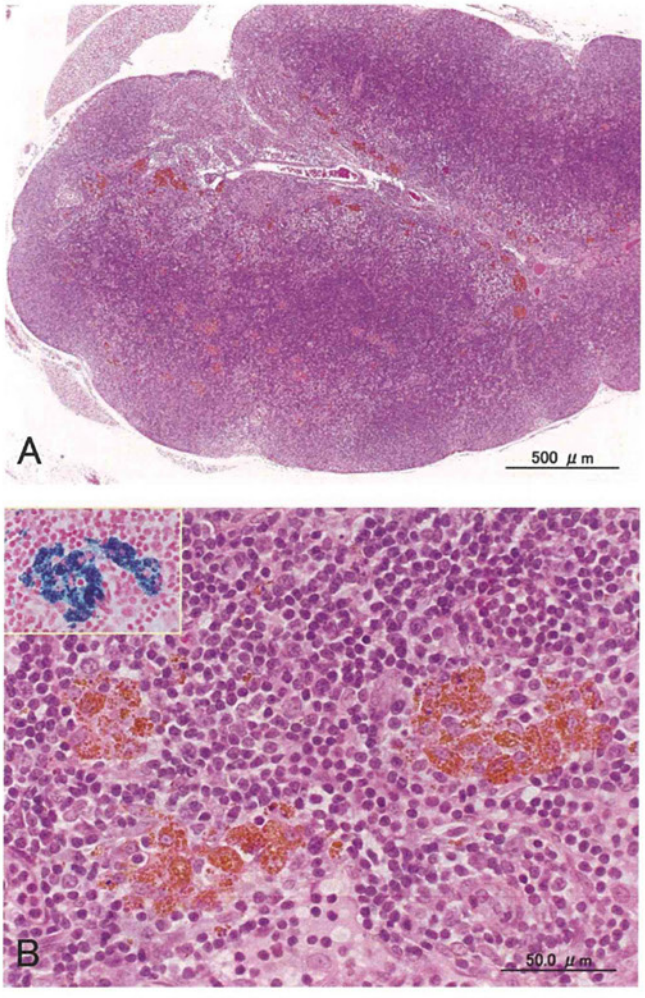

Fig. 5. Representative histologies of the parathymic lymph node (hematoxylin and eosin; inset, Berlin blue) from Fischer 344 rat treated with a single intratracheal spray instillation dose of 15.0 mg/kg body weight of magnetite on day 14. Infiltration of macrophages phagocytosing magnetite and deposits of magnetite particles are evident in rats given the middle dose.

ciated lymph node weights at the inhalation doses of 16.6 and 52.1 mg/m^3 [20]. Another report described data from an inhalation study in which male and female Han Wistar rats were exposed to a photocopying toner with an average particle size of 5.1 μm that contained 45–50% magnetite by inhalation for 6 hours/day, 5 days/week, for a total of 13 or 104 weeks[14]. The microscopic findings indicated a mild inflammatory response and infiltration of black-pigmented macrophages in the lungs and the tracheobronchial and mediastinal lymph nodes after 104 weeks of exposure at an inhalation dose of 16 mg/m^3. It is thus suggested that a longer time is required to develop apparent adverse effects, while the responses are generally less severe in the case of administration by inhalation than in the case of administration by instillation. Osier *et al.* compared the response of rats exposed by intratracheal inhalation to titanium dioxide particles with that of rats exposed to similar doses by intratracheal instillation[21]. Animals receiving particles through inhalation showed a decreased pulmonary response, measured by bronchoalveolar lavage parameters, in both severity and persistence when compared with those receiving particles through instillation. These results demonstrate a difference in pulmonary response to an inhaled *vs* an instilled dose, which may be due to differences in dose rate, particle distribution or altered clearance between the two methods. Several experiments have been performed in rats using quartz as a typical lung toxic particle in order to establish an appropriate bioassay for detection of lung damage after particle instillation[22]. The results of those experiments indicated that an intratracheal instillation bioassay system for detection of lung toxicity appeared to be suitable for rapid hazard identification. Even though inhalation is more similar to the exposure route of magnetite in humans than intratracheal instillation, studies using the latter route are still important.

Generally, the acute pulmonary response to foreign bodies is characterized by the inflammation to remove such substances and the resultant cellular debris. If this process is successfully accomplished, complete resolution can occur. On the other hand, if the injury caused by foreign bodies and the subsequent inflammation are severe and sustained due to the persistence of the substances, irreversible pulmonary damage may occur[23]. It is well known that, if the lung is not overloaded with dust, dust-laden macrophages on the alveolar surface migrate upward and are carried by the mucociliary "escalator" system up to the trachea to be cleared into the esophagus. However, when dust enters into the interstitial or subepithelial space of the lung, it becomes very difficult to clear from the lung[24]. Ultrafine particles that penetrate into the lung interstitium make contact with interstitial macrophages and other sensitive cell populations, which is likely to have powerful inflammatory effects that underlie the development of subsequent disease[25]. In the present study, magnetite-laden macrophages were seen not only in the alveolar space but also in the alveolar septa or interstitial space, even in the low-dose group, which indicates the possibility of severe injury resulting from intratracheal administration of magnetite.

In conclusion, these results show that intratracheally administered magnetite nanoparticles cause foreign body inflammatory and granulating lesions in the lung. Magnetite particles are accumulated mainly in the lung and partly translocated to the regional lymph nodes. These pulmonary responses occur in a dose-dependent manner in association with the increase in lung weight.

Acknowledgments: We would like to express our gratitude to Dr. Yukari Totsuka (Cancer Prevention Basic Research Project, National Cancer Center Research Institute, Tokyo, Japan) for arrangement of the supply of magnetite and helpful suggestions. We also thank Mr. Toshiyuki Hakata and the staff of Toda Kogyo Corp. (Otake, Hiroshima, Japan) for their generous supply of magnetite and its technical information. This work was supported in part by a Health and Labour Sciences Research Grant (awarded to Dai Nakae) from the Ministry of Health, Labour and Welfare (MHLW) of Japan.

References

1. Hood E. Nanotechnology: looking as we leap. Environ Health Perspect. **112**: A740–A749. 2004. [Medline] [CrossRef]
2. Torres-Martínez CL, Kho R, Mian OI, and Mehra RK. Efficient photocatalytic degradation of environmental pollutants with mass-produced ZnS nanocrystals. J Colloid Interface Sci. **240**: 525–532. 2001. [Medline] [CrossRef]
3. Lin BL, Shen XD, and Cui S. Application of nanosized Fe_3O_4 in anticancer drug carriers with target-orientation and sustained-release properties. Biomed Mater. **2**: 132–134. 2007. [Medline] [CrossRef]
4. Gang J, Park SB, Hyung W, Choi EH, Wen J, Kim HS, Shul YG, Haam S, and Song SY. Magnetic poly epsilon-caprolactone nanoparticles containing Fe_3O_4 and gemcitabine enhance anti-tumor effect in pancreatic cancer xenograft mouse model. J Drug Target. **15**: 445–453. 2007. [Medline] [CrossRef]
5. Kikumori T, Kobayashi T, Sawaki M, and Imai T. Anti-cancer effect of hyperthermia on breast cancer by magnetite nanoparticle-loaded anti-HER2 immunoliposomes. Breast Cancer Res Treat. **113**: 435–441. 2009. [Medline] [CrossRef]
6. Takada T, Yamashita T, Sato M, Sato A, Ono I, Tamura Y, Sato N, Miyamoto A, Ito A, Honda H, Wakamatsu K, Ito S, and Jimbow K. Growth inhibition of re-challenge B16 melanoma transplant by conjugates of melanogenesis substrate and magnetite nanoparticles as the basis for developing melanoma-targeted chemo-thermo-immunotherapy. J Biomed Biotechnol. **2009**: 457936. 2009. [Medline] [CrossRef]
7. Kawai N, Futakuchi M, Yoshida T, Ito A, Sato S, Naiki T, Honda H, Shirai T, and Kohri K. Effect of heat therapy using magnetic nanoparticles conjugated with cationic liposomes on prostate tumor in bone. Prostate. **68**: 784–792. 2008. [Medline] [CrossRef]
8. Ito A, Tanaka K, Honda H, Abe S, Yamaguchi H, and Kobayashi T. Complete regression of mouse mammary carcinoma with a size greater than 15 mm by frequent repeated hyperthermia using magnetite nanoparticles. J Biosci Bioeng. **96**: 364–369. 2003. [Medline]
9. Xia Z, Wang G, Tao K, Li J, and Tian Y. Preparation and acute toxicology of nano-magnetic ferrofluid. J Huazhong Univ Sci Technolog Med Sci. **25**: 59–61. 2005. [Medline] [CrossRef]
10. Jeng HA, and Swanson J. Toxicity of metal oxide nanoparticles in mammalian cells. J Environ Sci Health A Tox Hazard Subst Environ Eng. **41**: 2699–2711. 2006. [Medline] [CrossRef]
11. Chen BA, Jin N, Wang J, Ding J, Gao C, Cheng J, Xia G, Gao F, Zhou Y, Chen Y, Zhou G, Li X, Zhang Y, Tang M, and Wang X. The effect of magnetic nanoparticles of Fe(3) O(4) on immune function in normal ICR mice. Int J Nanomedicine. **5**: 593–599. 2010. [Medline] [CrossRef]
12. Pott F, Ziem U, Reiffer FJ, Huth F, Ernst H, and Mohr U. Carcinogenicity studies on fibres, metal compounds, and some other dusts in rats. Exp Pathol. **32**: 129–152. 1987. [Medline] [CrossRef]
13. Steinhoff D, Mohr U, and Hahnemann S. Carcinogenesis studies with iron oxides. Exp Pathol. **43**: 189–194. 1991. [Medline] [CrossRef]
14. Slesinski RS, and Turnbull D. Chronic inhalation exposure of rats for up to 104 weeks to a non-carbon-based magnetite photocopying toner. Int J Toxicol. **27**: 427–439. 2008. [Medline] [CrossRef]
15. Zhu MT, Feng WY, Wang B, Wang TC, Gu YQ, Wang M, Wang Y, Ouyang H, Zhao YL, and Chai ZF. Comparative study of pulmonary responses to nano- and submicron-sized ferric oxide in rats. Toxicology. **247**: 102–111. 2008. [Medline] [CrossRef]
16. Zhou YM, Zhong CY, Kennedy IM, and Pinkerton KE. Pulmonary responses of acute exposure to ultrafine iron particles in healthy adult rats. Environ Toxicol. **18**: 227–235. 2003. [Medline] [CrossRef]
17. Japanese Association for Laboratory Animal Science (JALAS) Guidelines for animal experimentation. Exp Anim. **36**: 285–288. 1987.
18. Driscoll KE, Costa DL, Hatch G, Henderson R, Oberdorster G, Salem H, and Schlesinger RB. Intratracheal instillation as an exposure technique for the evaluation of respiratory tract toxicity: uses and limitations. Toxicol Sci. **55**: 24–35. 2000. [Medline] [CrossRef]
19. Gad SC, and Weil CS. Statistics for toxicologist. In: Principles and Methods of Toxicology, 3rd ed. AW Hayes (ed). Raven Press, New York. 221-274. 1994.
20. Pauluhn J. Subchronic inhalation toxicity of iron oxide (magnetite, Fe(3) O(4)) in rats: pulmonary toxicity is determined by the particle kinetics typical of poorly soluble particles. J Appl Toxicol. **32**: 488–504. 2012. [Medline] [CrossRef]
21. Osier M, and Oberdorster G. Intratracheal inhalation vs intratracheal instillation: differences in particle effects. Fundam Appl Toxicol. **40**: 220–227. 1997. [Medline] [CrossRef]
22. Yokohira M, Kuno T, Yamakawa K, Hashimoto N, Ninomiya F, Suzuki S, Saoo K, and Imaida K. An intratracheal instillation bioassay system for detection of lung toxicity due to fine particles in F344 rats. J Toxicol Pathol. **22**: 1–10. 2009. [Medline]
23. Haschek WM, and Witschi HR. Respiratory system. In: Handbook of Toxicologic Pathology, Haschek WM, and Rousseaux CG (eds). Academic Press, San Diego. 761-827. 1991.
24. Lam CW, James JT, McCluskey R, and Hunter RL. Pulmonary toxicity of single-wall carbon nanotubes in mice 7 and 90 days after intratracheal instillation. Toxicol Sci. **77**: 126–134. 2004. [Medline] [CrossRef]
25. Donaldson K, Li XY, and MacNee W. Ultrafine (nanometre particle mediated lung injury. J Aerosol Sci. **29**: 553–560. 1998. [CrossRef]

International Journal of Nanomedicine

Dovepress

open access to scientific and medical research

Open Access Full Text Article

ORIGINAL RESEARCH

Magnetic nanoparticles of Fe_3O_4 enhance docetaxel-induced prostate cancer cell death

Akiko Sato[1]
Naoki Itcho[1]
Hitoshi Ishiguro[2,3]
Daiki Okamoto[1]
Naohito Kobayashi[4]
Kazuaki Kawai[5]
Hiroshi Kasai[5]
Daisuke Kurioka[1]
Hiroji Uemura[2]
Yoshinobu Kubota[2]
Masatoshi Watanabe[1]

[1]Laboratory for Medical Engineering, Division of Materials Science and Chemical Engineering, Graduate School of Engineering, Yokohama National University, Yokohama, Japan; [2]Department of Urology, Yokohama City University Graduate School of Medicine, Yokohama, Japan; [3]Photocatalyst Group, Kanagawa Academy of Science and Technology, Kawasaki, Japan; [4]Department of Molecular Pathology, Yokohama City University Graduate School of Medicine, Yokohama, Japan; [5]Department of Environmental Oncology, Institute of Industrial Ecological Sciences, University of Occupational and Environmental Health, Kitakyushu, Japan

Correspondence: Masatoshi Watanabe
Laboratory for Medical Engineering, Division of Materials Science and Chemical Engineering, Graduate School of Engineering, Yokohama National University, 79-5 Tokiwadai, Hodogayaku, Yokohama, Japan
Tel +81 453 393 997
Fax +81 453 393 997
Email mawata@ynu.ac.jp

Abstract: Docetaxel (DTX) is one of the most important anticancer drugs; however, the severity of its adverse effects detracts from its practical use in the clinic. Magnetic nanoparticles of Fe_3O_4 (MgNPs-Fe_3O_4) can enhance the delivery and efficacy of anticancer drugs. We investigated the effects of MgNPs-Fe_3O_4 or DTX alone, and in combination with prostate cancer cell growth in vitro, as well as with the mechanism underlying the cytotoxic effects. MgNPs-Fe_3O_4 caused dose-dependent increases in reactive oxygen species levels in DU145, PC-3, and LNCaP cells; 8-hydroxydeoxyguanosine levels were also elevated. MgNPs-Fe_3O_4 alone significantly reduced the viability of LNCaP cells; however, MgNPs-Fe_3O_4 enhanced the cytotoxic effect of a low dose of DTX in all three cell lines. MgNPs-Fe_3O_4 also augmented the percentage of DU145 cells undergoing apoptosis following treatment with low dose DTX. Expression of nuclear transcription factor κB in DU145 was not affected by MgNPs-Fe_3O_4 or DTX alone; however, combined treatment suppressed nuclear transcription factor κB expression. These findings offer the possibility that MgNPs-Fe_3O_4–low dose DTX combination therapy may be effective in treating prostate cancer with limited adverse effects.

Keywords: prostate cancer, magnetic nanoparticles, docetaxel, reactive oxidative species

Introduction

Prostate cancer is the most common cancer affecting men, and the second leading cause of cancer death in the United States.[1] The incidence and mortality rates of prostate cancer vary greatly among different geographic areas and ethnic groups. Although the incidence of prostate cancer in Japan remains low compared with that in the United States, it has been increasing in recent years. However, by 2020, prostate cancer is projected to surpass stomach cancer as the most frequently diagnosed cancer in Japanese men.[2]

Several management options are available when prostate cancer is diagnosed at an early stage, including watchful waiting, surgery, cryosurgery, radiation therapy, and hormonal therapy. For advanced prostate cancers, surgical or medical ablation of androgens is regarded the optimal first-line treatment. In most patients treated by androgen deprivation, disease progression will continue until reaching a stage referred to as castration-resistant prostate cancer (CRPC). Progression to a hormonal refractory state is a complex process, involving both selection and outgrowth of preexisting clones of androgen-independent cells as well as adaptive upregulation of genes that help cancer cells survive and grow after androgen ablation.[3]

Although the effects of several anticancer drugs for prostate cancer have been evaluated in vitro and in animal experiments in vivo, most have little or no impact

submit your manuscript | www.dovepress.com
Dovepress
40766